2017

Hydrothermal Atomic Force Microscopy Investigation of Barite Growth: The Role of Spectator Ions in Elementary Step Edge Growth Kinetics and Hillock Morphology

Sarah A. Jindra
Wright State University

HYDROTHERMAL ATOMIC FORCE MICROSCOPY INVESTIGATION OF BARITE GROWTH: THE ROLE OF SPECTATOR IONS IN ELEMENTARY STEP EDGE GROWTH KINETICS AND HILLOCK MORPHOLOGY

A thesis submitted in partial fulfillment
of the requirements for the degree of
Master of Science

By

SARAH A. JINDRA
B.S., Bowling Green State University, 2015

2017
Wright State University

WRIGHT STATE UNIVERSITY

GRADUATE SCHOOL

July 31, 2017

I HEREBY RECOMMEND THAT THE THESIS PREPARED UNDER MY SUPERVISION BY Sarah A. Jindra ENTITLED Hydrothermal Atomic Microscopy Investigation of Barite Growth: The Role of Spectator Ions in Elementary Step Edge Growth Kinetics and Hillock Morphology. BE ACCEPTED IN PARTIAL FULFILLMENT OF THE REQUIREMENTS FOR THE DEGREE OF Master of Science.

_____
Steven Higgins, Ph.D.
Department of Chemistry
College of Science and Mathematics

_____
David Grossie, Ph.D., Chair
Department of Chemistry
College of Science and Mathematics

Committee on Final Examination

_____
Steven Higgins, Ph.D.

_____
Ioana Sizemore, Ph.D.

_____
David Dolson, Ph.D.

_____
Robert E. W. Fyffe, Ph.D.,
Vice President for Research and
Dean of Graduate School

ABSTRACT

Jindra, Sarah A. M.S. Department of Chemistry, Wright State University, 2017. Hydrothermal Atomic Microscopy Investigation of Barite Growth: The Role of Spectator Ions in Elementary Step Edge Growth Kinetics and Hillock Morphology.

To better understand the role of spectator ions in barite growth, the kinetics of step edge growth on barite (001) surfaces were studied under various salt solutions. Hydrothermal Atomic Force Microscopy (HAFM) was used to investigate the effect of background electrolytes (NaCl, NaBr and $NaNO_3$) as a function of saturation index and ionic strength (*I*) on barite growth sourced at dislocations at 108 ºC. Results show that hillock morphology is affected by *I*, as well as type of anion, where the prevalence of steps aligned on the [010] direction is highest under Cl^-. There is a modest increase in kinetic coefficient of 55-130% with a ten-fold increase in *I* for each salt. In comparing the kinetic coefficients of the salts at low ionic strength (0.01 M), there is a moderate difference, suggesting that the anion may play a role in barium attachment.

TABLE OF CONTENTS

LIST OF FIGURES

LIST OF TABLES

I. INTRODUCTION

Sparingly-soluble minerals, such as barite ($BaSO_4$), play key roles in geological and industrial systems. Specifically, the growth of barite occurs in various geologic settings such as oceans,[1] as well as in off-shore drilling operations where barite scale formation can be problematic and in industrial settings such as reverse osmosis systems.[2] Understanding barite growth is significant in combating unwanted growth and utilizing growth for contamination uptake. [3] Furthermore, barium has been found as a contaminant in natural gas drilling waste waters which are then treated at municipal waste water plants. [4,5] The efficacy of clean-up or treatment technologies for this waste water, relying on the limited solubility of barium sulfate, will be impacted by the kinetics of barite crystal growth and the conditions under which barite grows.

Mineralization of barium sulfate can be explained by crystal growth theory, which describes the spread of a crystal face by crystal units (e.g., Ba^{2+} and SO_4^{2-}) attaching and detaching randomly and frequently to step edges. Under relatively low supersaturation, the crystal units attach to/detach from kink sites, which exist along step edges due to thermal fluctuations as well as nucleation events(Appendix A).[6-8] At higher supersaturation, crystal growth rates are governed by the probability of two-dimensional nucleation and other step advancement mechanisms, while near equilibrium environments lead to growth through attachment of solute ions to existing step edges.[6] Crystal growth theory demonstrates that elementary step edge growth rates for an AB-type crystal, such as barite, when cation and anion activities are near unity can be described by:[6-8]

$$V_s = \beta V_m(\{Ba^{2+}\} - \{Ba^{2+}\}_{eq}) \qquad (1)$$

where β (cm/s) is the rate coefficient, V_m is the molar volume of barite, $\{Ba^{2+}\}$ is barium activity (M) and $\{Ba^{2+}\}_{eq}$ is activity at equilibrium (1.8 x 10^{-5} M at 108 ºC). [6,9] β is described by the frequency of molecular oscillations, size of attaching species, steric factors, activation energy for attachment and kink density.[9] Step velocities on barite (001)[10] (and celestite (001))[11] surfaces were shown to be maximized when the ratio of barium (or strontium) to sulfate activities are near unity.

Barite growth has been studied under different solution compositions such as changing pH, where two-dimensional and three-dimensional barite nucleation rates increased with an increase in pH above pH ~ 9-10.[12] Previous studies on barite demonstrate that barite growth is anisotropic and that growth morphology on a crystal is governed by the bulk crystal structure[13] and by understanding the effect of anisotropy and symmetry, models can be used to predict crystal growth.[14] Under high ionic strength and high supersaturation, barite hillocks[15] as well as bulk barite crystals were found to elongate in the [010] direction.[16] The [010] step direction also forms in hillocks grown under low ratios of barium to sulfate activity and under very dilute (1 mM) $NaNO_3$ solutions.[10] Growth hillocks sourced by screw dislocations on the barite(001) surface establish a morphology that is indicative of the slowest growing step edges under the prevailing conditions. Prior room temperature studies by Risthaus et al.[17] and Becker et al.[18] concluded that the presence of high concentrations of NaCl stabilized steps parallel to the [010] direction through the adsorption of Na^+ and Cl^- ions to the [010] steps. At lower NaCl concentrations, these steps were destabilized by the presence of parallel dipoles along the step edge and therefore, [010] step directions were not observed.

Barite (001) growth under different background electrolytes also has been studied by Kowacz et al. who found that the background electrolyte and ionic strength affected island spreading rates based on how well the spectator ions are able to structure water around the ions of the crystal unit.[19] He et al. reported that, in general, with an increase in ionic strength there was a decrease in induction time for homogenous nucleation (increased growth rate) except at higher ionic strengths of NaCl (4-6 *m*) where there was a slight increase in induction time (growth rate decreases). [20] He et al. hypothesized that there was a slight decrease in growth at these higher ionic strengths of NaCl due to Na^+ incorporating itself into the crystal lattice.[20] In general, it was reported that with an increase in ionic strength there is an increase in barite crystal growth rates. [15,17,18]

In regard to the kinetics of elementary step edge advancement, there is little available data in the literature on how the electrolyte concentration impacts individual step edges. Previous studies report island spreading rates on barite (001) surfaces, however island spreading consists of the summation of two opposing and crystallographically inequivalent step edge velocities, therefore it is not known how the individual steps on barite behave as a function of solution composition, and there has been little quantitative investigation of barite crystal growth kinetics with different background electrolytes. [17,19,21] To test the quantitative relationship between elementary step velocity and ionic strength, as well as to test for a possible role of the electrolyte anion in the step kinetics and growth hillock morphology, we conducted *in-situ* Hydrothermal Atomic Force Microscopy (HAFM) experiments at 108 ºC.

II. METHOD AND MATERIALS

Materials and Solution Preparation

Stock solutions of barium chloride (Aldrich, 99.999%), sodium sulfate (Aldrich, 99.99%), sodium chloride (Aldrich, 99.999%), sodium nitrate (Aldrich, 99.995%) and sodium bromide (Alfa Aesar, 99.99%) were prepared with deionized water (Millipore, resistivity = 18.2 MΩ•cm). The barite crystals contained less than 7.0 x 10^{-2} mol/mol Ba% trace metal impurities.[10] Solution speciation was calculated using PHREEQC along with the LLNL thermodynamic database which includes a K_{sp} for barite of $10^{-9.48}$ at 108 °C.[22] In this database, activities were calculated using an extension of the Debye-Hückel model that includes the B-dot parameter.[23] Solution compositions calculated at 108 °C are listed Table 1 and solution compositions are precise up to ±2% based on random errors in micropipettes. The solution compositions are calculated to have a pH of ~ 6. Uncertainties were not estimated for barium activities or saturation index. Saturation index, as defined by Eq.2:

$$SI = \log \frac{\{Ba^{2+}\}\{SO_4^{2-}\}}{K_{sp,barite}} \quad (2)$$

varied from 0 to 0.52 for each set of electrolyte solutions, where $\{i\}$ represents the activity of species i.

During the course of investigations, we discovered that some supersaturated solutions, such as 0.1 M NaCl with r >1, where r is the ratio of barium molality to sulfate

molality, were unstable on a timescale of minutes, possibly due to homogeneous nucleation of barite or heterogeneous nucleation on suspended particulates in unfiltered solutions (See Appendix B). The precipitation would decrease the saturation state and barium activity by an unknown amount. To address these concerns, stock solutions were filtered using 0.2 μm filters (Millipore) for some of the experiments (e.g., all of the NaBr stock solutions were filtered and the majority of 0.01 M $NaNO_3$ solutions were prepared from filtered stock solutions). Filtering of the stock solutions was found to have a negligible effect on the stability of the supersaturated solutions. Results of solution stability investigations appear in Appendix B.

HAFM Experiments

Barite samples were cleaved with a razor blade to expose the (001) face. Particles generated during the cleaving process were removed with N_2 before the sample was secured with a gold wire onto the sample disk in the HAFM fluid cell.[24] (See Appendix A for more information on the HAFM). Barite, which crystallizes with space group *Pnma*, displays perfect cleavage on (001) surfaces that are charge-neutral due to the equal populations of cations and anions exposed on this surface (see Bracco et al. and Appendix A for additional details on barite (001) crystallography).[10] The sample was then covered with deionized water at room temperature during set up. The experiments were performed at 108 °C and 4.1 atm (N_2), and studies were performed at a solution flow rate of 12.5 mL/hr, which does not limit the rate of crystal growth (See Appendix B and Bracco et al.).[10]

Table 1: Solution composition for HAFM barite growth experiments.

Table Note: Concentration of $BaCl_2$ and Na_2SO_4 stock solutions is 0.0100 M for all experiments.

Experiment Number	**Runs**	**mL Na_2SO_4 Added**	**mL $BaCl_2$ Added**	**mL Background Electrolyte Added**	**$[Ba^{2+}]$ (x 10^{-5})**	**$[SO_4^{2-}]$ (x 10^{-5})**	**$\{Ba^{2+}\}$ (x 10^{-5}) (M)**	***SI***	**r ($[Ba^{2+}]/[SO_4^{2-}]$)**	***I*** **(x 10^{-2}) (M)**	**Average Velocity (nm/s)**	**Average Velocity Standard Deviation**
1	Cl- 1C	0.17	0.17	49.66	3.4	3.3	2.1	0.09	1.03	1.03	0.43	0.02
1	Cl-2C	0.19	0.19	49.62	3.8	3.7	2.3	0.19	1.03	1.03	0.65	0.04
1	Cl-3C	0.22	0.22	49.56	4.4	4.2	2.7	0.32	1.03	1.03	1.1	0.3
1	Cl-4C	0.25	0.25	49.5	5.0	4.8	3.1	0.43	1.03	1.04	1.4	0.1
1	Cl-5C	0.27	0.27	49.46	5.4	5.2	3.3	0.5	1.03	1.04	2.0	0.1
1	Cl-1B	0.29	0.27	49.44	5.3	5.2	2.1	0.11	1.02	4.95	0.29	0.02
1	Cl-2B	0.32	0.3	49.38	5.9	5.7	2.4	0.2	1.03	4.95	0.83	0.04
1	Cl- 3B	0.37	0.35	49.28	6.8	6.6	2.8	0.33	1.04	4.94	1.1	0.1
1	Cl-4B	0.4	0.38	49.22	7.4	7.1	3.0	0.4	1.04	4.94	1.4	0.1
1	Cl-5B	0.45	0.43	49.12	8.4	8.0	3.4	0.5	1.05	4.94	2.2	0.1
1	Cl-0A	0.37	0.33	49.3	6.9	6.7	2.0	0.05	1.03	9.80	0.31	0.04
1	Cl-2A	0.45	0.4	49.15	7.7	7.6	2.5	0.22	1.01	9.77	1.1	0.1
1	Cl-3A	0.5	0.45	49.05	8.6	8.4	2.8	0.32	1.03	9.76	1.9	0.2
1	Cl-4A	0.55	0.5	48.95	9.6	9.3	3.1	0.4	1.04	9.75	2.2	0.2
1&2	Cl-5A	0.6	0.55	48.85	11	10	3.4	0.48	1.04	9.73	2.5	0.6

The concentration for 0.01 M NaCl is 0.0102 M, 0.05 M NaCl is 0.0501 M, 0.1 M NaCl is 0.100 M.

Experiment Number	Runs	mL Na_2SO_4 Added	mL $BaCl_2$ Added	mL Background Electrolyte Added	$[Ba^{2+}]$ (x 10^{-5})	$[SO_4^{2-}]$ (x 10^{-5})	$\{Ba^{2+}\}$ (x 10^{-5}) (M)	*SI*	r ($[Ba^{2+}]/[SO_4^{2-}]$)	*I* (x 10^{-2}) (M)	Average Velocity (nm/s)	Average Velocity Standard Deviation
2-3	Br-1C	0.175	0.17	49.655	3.4	3.4	2.1	0.11	1.02	1.06	0.5	0.1
3	Br-2C	0.2	0.195	49.605	3.9	3.8	2.4	0.22	1.02	1.06	0.8	0.1
3	Br-3C	0.22	0.22	49.56	4.4	4.2	2.7	0.32	1.04	1.06	0.9	0.1
3	Br-4C	0.25	0.245	49.505	4.9	4.8	3.0	0.42	1.02	1.07	1.0	0.3
3	Br-5C	0.28	0.27	49.45	5.4	5.4	3.3	0.51	1.01	1.07	1.2	0.2
2	Br-1B	0.29	0.26	49.45	5.2	5.2	2.1	0.1	1.01	5.03	0.7	0.1
2	Br-2B	0.32	0.29	49.39	5.8	5.7	2.3	0.19	1.02	5.03	0.7	0.1
2	Br-3B	0.37	0.33	49.30	6.6	6.6	2.7	0.31	1.01	5.03	1.5	0.2
2	Br-4B	0.41	0.37	49.22	7.4	7.3	3.0	0.4	1.02	5.02	1.6	0.1
2	Br-5B	0.46	0.41	49.13	8.2	8.2	3.3	0.5	1.01	5.02	2.0	0.2
3	Br- 1A	0.39	0.33	49.28	6.6	6.6	2.1	0.09	1.01	9.93	0.9	0.1
2	Br-2A	0.44	0.37	49.186	7.5	7.4	2.4	0.19	1.00	9.98	1.6	0.3
2&3	Br-3A	0.49	0.42	49.094	8.4	8.2	2.7	0.29	1.02	9.91	2.2	0.4
2	Br-4A	0.55	0.47	48.98	9.4	9.3	3.0	0.39	1.02	9.95	2.0	0.2
2	Br-5A	0.62	0.53	48.853	11	10	3.4	0.49	1.02	9.93	2.2	0.2

Step velocities were averaged with solutions that required another run and often new stock solution needed to be made. The actual concentrations of 0.01 M NaBr is 0.0105 M, 0.05 M NaBr is 0.0505 M NaBr and 0.1 M NaBr is 0.101 M.

Experiment Number	Runs	mL Na_2SO_4 Added	mL $BaCl_2$ Added	mL Background Electrolyte Added	$[Ba^{2+}]$ (x 10^{-5})	$[SO_4^{2-}]$ (x 10^{-5})	$\{Ba^{2+}\}$ (x 10^{-5}) (M)	*SI*	r ($[Ba^{2+}]/[SO_4^{2-}]$)	*I* (x 10^{-2}) (M)	Average Velocity (nm/s)	Average Velocity Standard Deviation
1	NO_3-1C	0.17	0.175	49.655	3.4	3.3	2.1	0.09	1.02	1.02	0.27	0.02
2 & 3	NO_3-2C	0.195	0.2	49.605	3.8	3.8	2.4	0.21	1.02	1.02	0.8	0.2
1	NO_3-3C	0.22	0.225	49.555	4.3	4.2	2.7	0.31	1.02	1.02	0.74	0.04
1	NO_3-4C	0.245	0.25	49.505	4.8	4.7	3.0	0.41	1.02	1.02	1.04	0.05
1	NO_3-5C	0.275	0.28	49.445	5.4	5.3	3.3	0.51	1.01	1.02	1.5	0.1
1	NO_3-0B	0.260	0.275	49.465	4.8	4.6	1.9	0.01	1.03	4.99	0.22	0.01
1	NO_3-2B	0.320	0.340	49.340	5.9	5.7	2.4	0.2	1.04	4.98	1.0	0.1
2	NO_3-3B	0.360	0.380	49.260	6.6	6.4	2.7	0.3	1.03	4.96	1.5	0.3
2	NO_3-4B	0.410	0.430	49.160	7.5	7.3	3.0	0.41	1.02	4.97	1.9	0.3
1	NO_3-5B	0.460	0.485	49.055	8.4	8.2	3.4	0.51	1.03	4.97	1.9	0.1
2 & 3	NO_3-1A	0.4	0.42	49.18	6.8	6.7	2.2	0.11	1.01	9.90	0.8	0.1
2	NO_3-2A	0.45	0.47	49.08	7.6	7.6	2.4	0.21	1.00	9.88	1.9	0.2
2	NO_3-3A	0.51	0.54	48.95	8.7	8.6	2.8	0.33	1.02	9.87	2.4	0.3
2	NO_3-4A	0.56	0.59	48.85	9.5	9.4	3.1	0.41	1.01	9.85	2.1	0.3
2	NO_3-5A	0.62	0.65	48.73	11	11	3.4	0.49	1.00	9.83	3.5	0.4

The actual concentrations of 0.01 $NaNO_3$ is 0.0100 M, 0.05 M $NaNO_3$ is 0.0500 M and 0.1 M $NaNO_3$ is 0.0998 M.

Pt-Ir-coated Si cantilevers ((Nanosensors-PPPCONTPt, coating on both sides) with a nominal spring constant in the range from 0.02 to 0.77 N/m were used for imaging in contact mode.

The HAFM has a fluid jet which vertically impinges on the surface near the cantilever, which leads to rapid changes in solution composition during solution changes. As such, step velocities were typically measured (within 1 to 5 minutes after the solution entered the fluid cell) to ensure any solution instabilities (Appendix B) did not affect step velocity measurements. The morphologies of the growth hillocks were observed after about 20 minutes of growth so that the steps made by the previous solution would have advanced out of the field of view. Previous studies[10] allowed 30 minutes or more of new solution flow to take place before measuring step velocities in lower ionic strength solutions, however our detailed investigations at higher ionic strengths demonstrate solution instability in certain cases (See Appendix B), thus making it necessary to collect step growth data as soon as practicable after solution preparation. For the majority of the experiments reported here, the time elapsed from the preparation of the solution to the data collection was approximately 10 minutes. Step velocities were measured using distortions of growth hillock morphology caused by the motion of step edges during image acquisition. The method, described by Land et al., relates the observed angle between step edges and the image horizontal in both upward and downward scanned images to the velocity of the step edges.[25] The relationship is given in Eq. 3:

$$v = \frac{RS}{2N}(cot\theta_D - cot\theta_U)sin\left[cot^{-1}\left(\frac{cot\theta_D + cot\theta_U}{2}\right)\right] \quad (3)$$

where R is the linescan rate of the image in Hz, S is the scan size (nm) and N is the number of lines in the collected image and θ_D and θ_U are the angles observed in downward and upward scanned images, respectively. Propagation of error from the angle measurements to step velocities can be found in Appendix B. To study how the anion of the background electrolyte affects barite growth, we investigated various Na electrolyte solutions (NaCl, $NaNO_3$ and NaBr) at three ionic strengths ($I = 0.01, 0.05$ and 0.1 M) and at up to 5 different saturation indexes for each ionic strength.

Hillock Morphology Index:

To facilitate comparison of barite hillock morphologies obtained in different solutions, we will compare the lengths of steps oriented parallel to [010] and ⟨120⟩ directions to define the Hillock Morphology Index (HMI), which is equal to the ratio of [010] step length to the ⟨120⟩ step length. The barite hillock is a complex hillock with bilayer and monolayer step segments and measurements of step lengths are taken on the bilayer and monolayer steps as shown in Figure 1B. The step lengths were measured on steps close to the top of the hillock in order to be certain that the measurements reflected the effect of current, rather than a previous, solution. On complex hillocks, such as one that has two hillocks competing next to each other, step lengths were measured on steps that were not directly affected by the competing hillock.

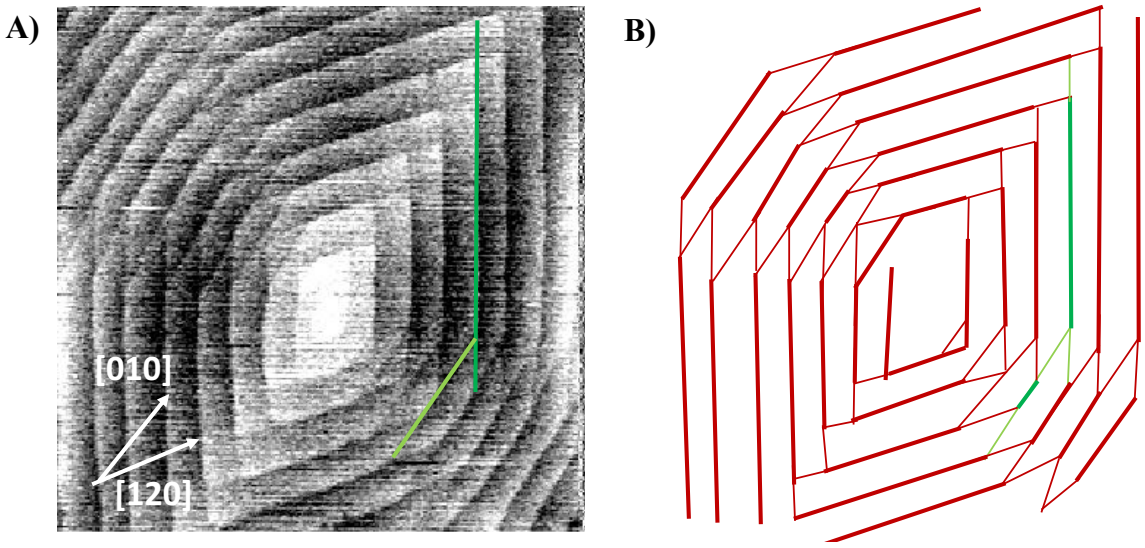

Figure 1: Example of measurements of [010] and ⟨120⟩ step lengths on a hillock under 0.1 M NO_3 (*SI* =0.11) used to find the ratio of the lengths (a) and (b) shows a barite hillock consisting of [010] and [120] bilayer steps (dark lines) and monolayer (light lines) with a [120] step and [010] step highlighted in green to demonstrate where measurements of step length would be collected.

III. RESULTS

When barite (001) surfaces are exposed to modestly supersaturated solutions (i.e., $0 < SI < 1$), growth at screw dislocation outcroppings results in spiral growth hillocks similar to the hillock shown in Figure 1. When these supersaturated solutions contain NaCl as the background electrolyte, the morphology of the growth hillocks are found to depend on the concentration of NaCl (Figure 2). Hillocks grown in solutions of 0.05 M and 0.1 M NaCl are comprised of [010] and ⟨120⟩ steps (Figure 2A-F), whereas hillocks grown in 0.01 M NaCl are primarily composed of ⟨120⟩ steps (Figure 2 (G-I)). For hillocks under 0.05 M NaCl and 0.1 M NaCl, the morphology did not strongly depend on the solution supersaturation (Figure 2 (A-F)).

In an effort to determine if the anion of the background electrolyte plays a role in the observed hillock morphology, solutions with NaBr in place of NaCl were investigated. Figure 3 shows the topographic images of barite hillocks grown under NaBr solutions with the appearance of ⟨120⟩ steps in all conditions as was the case for NaCl. Hillocks developed in 0.1 M NaBr solutions (Figure 3 (A-C)) consist [010] and ⟨120⟩ steps while those developed in 0.01 M NaBr are composed of only ⟨120⟩ steps (Figure 3 (G-I)). Figure 3 (E-F) shows hillocks under 0.05 M solutions, and the presence of [010] steps far from the center of the hillocks is evident, however, these [010] steps are the result of growth in previous solutions. In general, the effect of NaBr on the hillock morphology is not

significantly different from the effects of NaCl, however, the [010] step is more prominent in NaCl solutions when compared to the NaBr solutions at higher *I*.

As a comparison to the NaCl and NaBr background electrolytes, solutions containing $NaNO_3$ were utilized in growth experiments with ⟨120⟩ steps prevalent in all solutions made from this salt (Figure 4). The [010] steps are only noticeable in hillocks grown under 0.1 M $NaNO_3$ solutions. This is unlike the hillocks under NaCl and NaBr solutions, in which the presence of [010] steps are also found under 0.05 M solutions (Figure 2 D-F, Figure 3 D). As was the case for both NaCl and NaBr solutions, in $NaNO_3$, supersaturation did not influence the hillock morphology as it pertains to the presence or absence of [010] steps. The primary effect of supersaturation was to alter the step density.

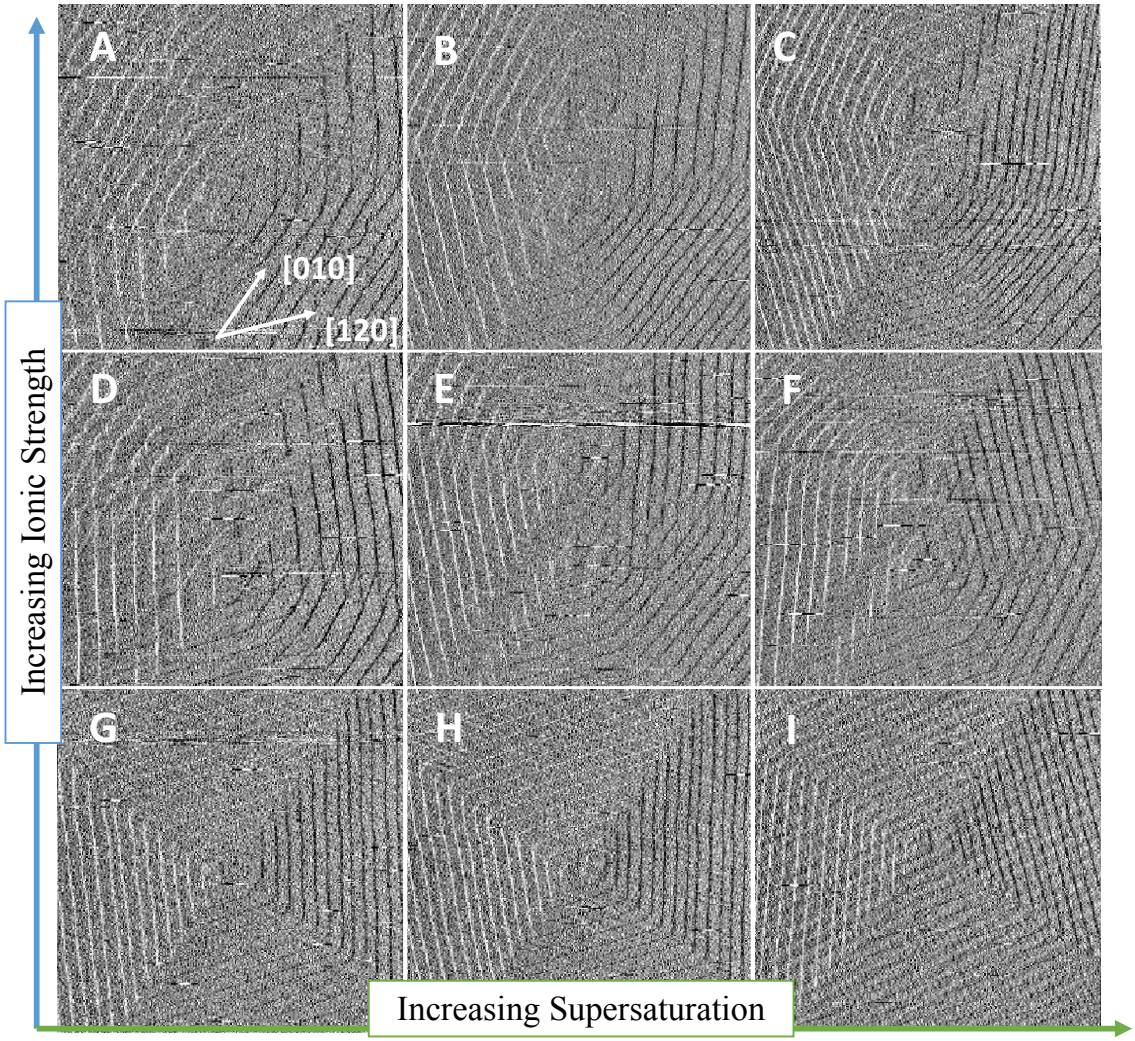

Figure 2: *In-situ* HAFM error signal images (giving appearance of illumination source on the left) with increasing ionic strength (I) versus increasing saturation index for NaCl solutions. In A, the direction of the [010] and [120] steps are labeled. Hillocks in A, B and C developed in 0.1 M NaCl solutions (*SI*~0.05, 0.32, and 0.48, respectively); D, E and F developed in 0.05 M NaCl solutions (*SI* ~ 0.11, 0.33 and 0.5, respectively) and G, H, and I are from 0.01 M NaCl solutions (*SI*~ 0.09, 0.32 and 0.5, respectively). Lateral images dimensions are 3.3 μm x 3.3 μm.

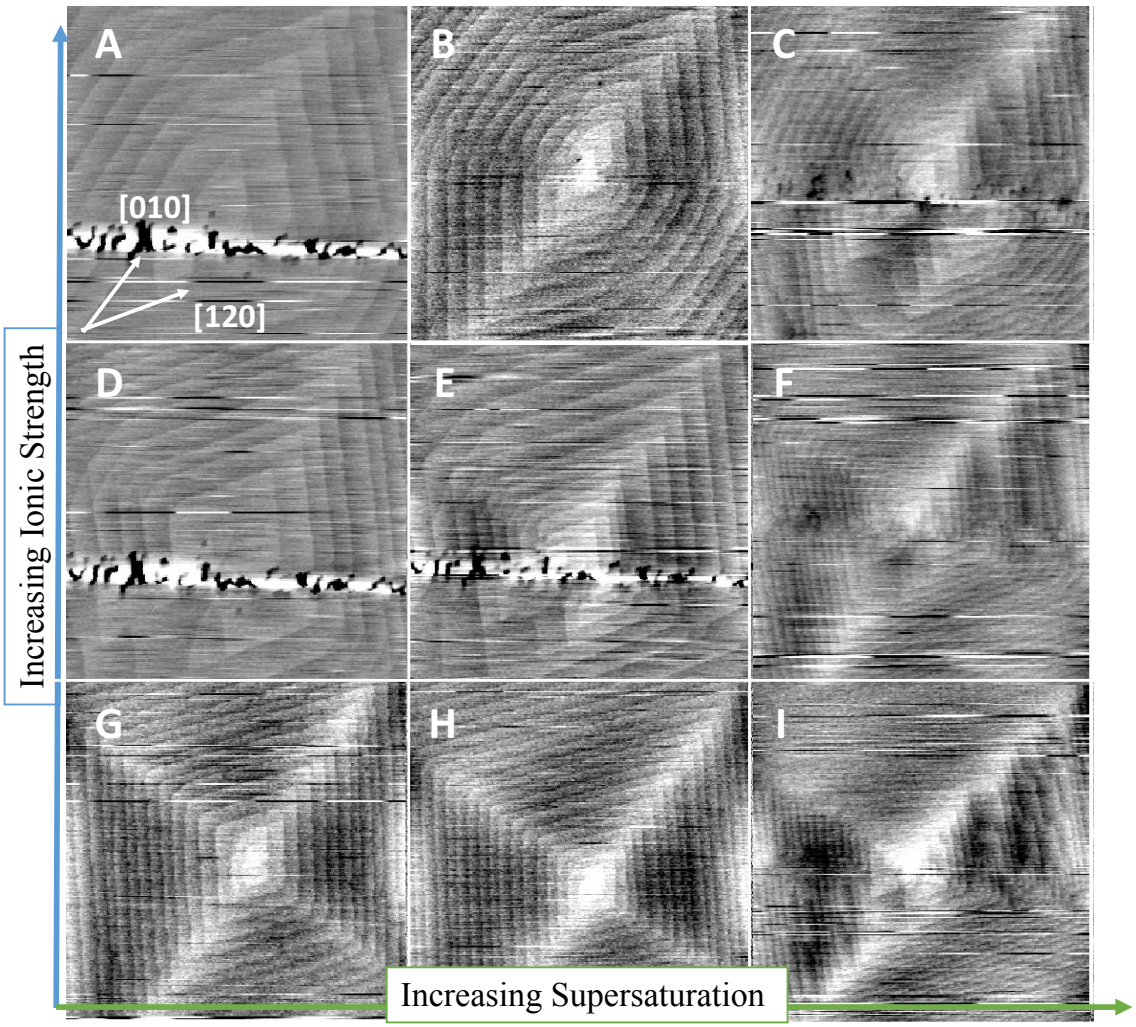

Figure 3: *In-situ* HAFM topographical images with increasing ionic strength (I) versus increasing saturation index for NaBr solutions. In A, the direction of the [010] and [120] steps are labeled. Hillocks in A, B and C developed in 0.1 M NaBr solutions (*SI*~ 0.09, 0.29, and 0.49, respectively); D, E and F developed in 0.05 M NaBr solutions (*SI*~ 0.1, 0.31, and 0.5, respectively). Lateral image dimensions for B, G and H are 2.6 μm x 2.6 μm, images C, F, and I are 4.25 μm x 4.25 μm and images A, D, and E are 5μm x 5 μm.

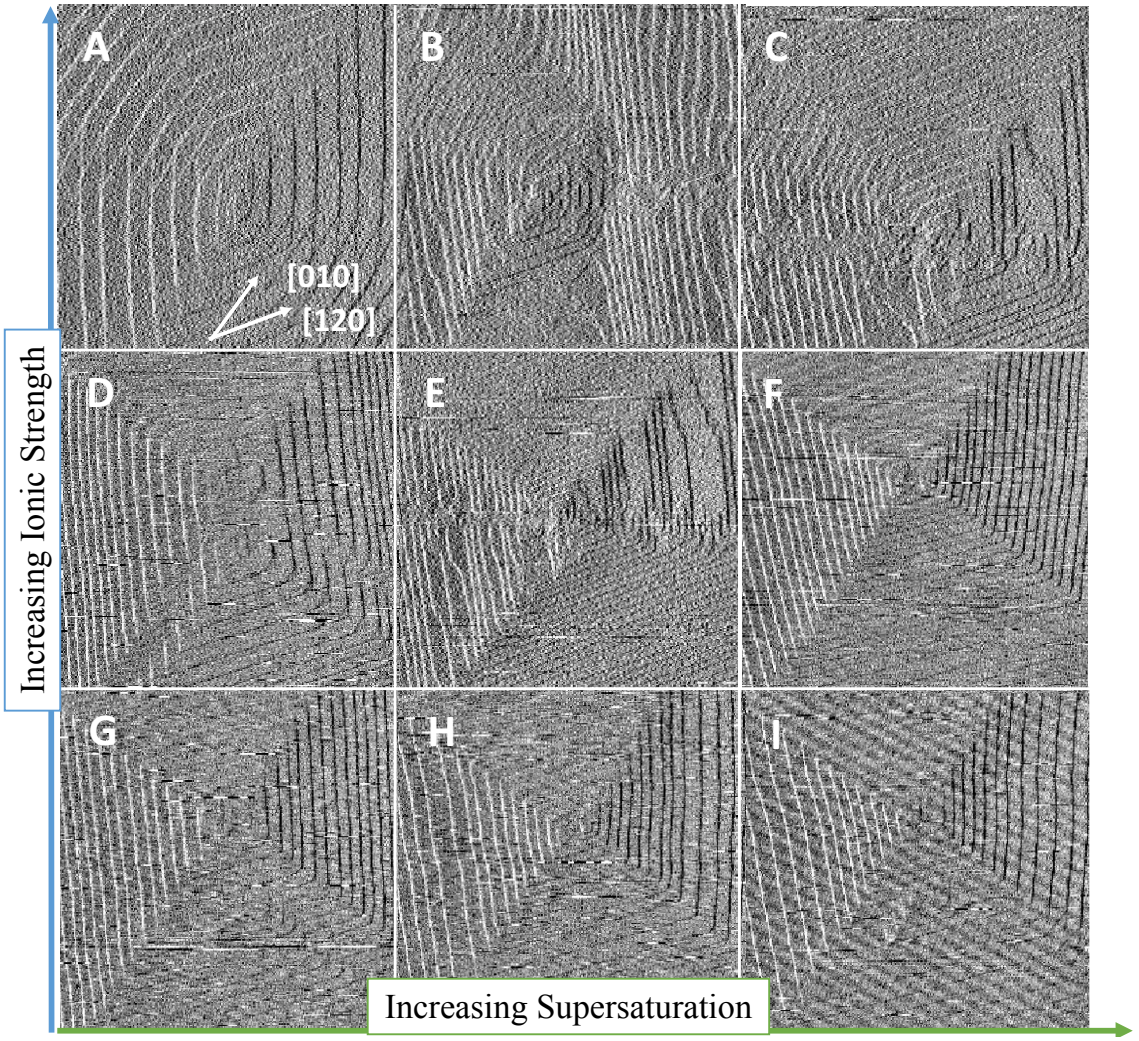

Figure 4: *In-situ* HAFM error signal images (giving appearance of illumination source on the left) with increasing ionic strength (I) versus increasing saturation index for $NaNO_3$ solutions. In A, the direction of the [010] and [120] steps are labeled. Hillocks in A, B and C are due to 0.1 M $NaNO_3$ solutions (*SI*~ 0.11, 0.41, and 0.49, respectively); D, E and F are from 0.05 M $NaNO_3$ solutions (*SI*~ 0.01, 0.41 and 0.51, respectively) and G, H, and I are from 0.01 M $NaNO_3$ solutions (*SI*~ 0.09,0.41 and 0.51, respectively). Lateral image dimensions for image A are 3.2 μm x 3.2 μm, image B are 3.9 μm x 3.9 μm, image C are 2.6 μm x 2.6 μm, images D, F-I are 3.3 μm x 3.3 μm and image E are 4.25 μm x 4.25 μm.

To better describe the morphology of the hillocks in different solutions, the HMI was determined for hillocks in which the [010] steps were present (HMI > 0). For hillocks where [010] steps were absent, HMI = 0. While the HMI allows for the hillock morphology to be described quantitatively, uncertainties were not estimated due to the possible influence of the complex screw dislocation outcroppings on the shape of the hillocks. The HMI number in Figure 5 indicates that hillocks under 0.1 M NaCl solutions are dominated by both [010] and ⟨120⟩ step directions, which results in more elongation of the hillock parallel to [010] than solutions of lower *I*. There is an absence of the [010] direction for 0.01 M NaCl, NaBr and $NaNO_3$. Under 0.1 M NaBr solutions, all five hillocks formed under this ionic track have HMI numbers assigned while 0.05 M NaBr showed the presence of [010] steps only in lower supersaturation solutions (Figure 5). The HMI numbers for 0.1 M $NaNO_3$ range have a lower range than 0.1 M NaCl and 0.1 M NaBr HMI numbers (Figure 5). In summary, the HMI appears to increase with increasing *I* while HMI increases in the order $NO_3^- < Br^- < Cl^-$.

In investigating the effect of anions on kinetic coefficients, ⟨120⟩ step velocities for each ionic strength of the background electrolyte is plotted versus barium activity. Figure 6A shows the quantitative data for ⟨120⟩ step velocities as a function of barium activity at the three different ionic strengths of NaCl. Each data set at a given ionic strength was fit to Eqn. (1) using linear least-squares method and data point weighting based on the size of the individual error bars, which represent the standard deviations of the step angle measurements that were subsequently converted to estimates of the standard deviation of the step velocities as described in Appendix A. Kinetic coefficients for each salt and ionic strength are shown in Table 2. Table 3 shows statistical comparisons of the kinetic

coefficients where p is the probability value of the statistic being true and α is the standard that is set so that if $p > \alpha$ then the null hypothesis is true. The null hypothesis is that the differences in kinetic coefficients are not due to chance, but if $p < \alpha$, where $\alpha = 0.1$, then the null hypothesis is rejected and the comparisons are statistically different with 90% confidence. There is strong evidence to suggest there is a significant difference in kinetic coefficients (i.e., slopes) between 0.01 M NaCl and 0.1 M NaCl. The point estimate for this difference was 0.14 cm/s which corresponds to a 55% increase in β from $I = 0.01$ M to $I = 0.1$ M NaCl. There is no statistical difference in kinetic coefficients between 0.01 M and 0.05 M NaCl and likewise no statistical difference between 0.05 M and 0.1 M NaCl (Table 3). Details of the statistical analysis behind Table 2 and Table 3 are in Appendix B.

The ⟨120⟩ step velocity measurements at the three different NaBr ionic strengths demonstrate that the slope of 0.01 M NaBr is different than 0.05 M and 0.1 M NaBr (Figure 6B). In comparing the kinetic coefficients of the different ionic strengths of NaBr (Table 2), there is strong evidence to support that there is a significant difference in the kinetic coefficients between 0.01 M and 0.05 M NaBr. The point estimate for this difference is 0.10 cm/s which corresponds to a 84% increase in β from $I = 0.01$ M to $I = 0.05$ M NaBr . There is also strong evidence to support that there is a significant difference in the kinetic coefficients between 0.01 M NaBr and 0.1 M NaBr. The point estimate for this difference in kinetic coefficient is 0.095 cm/s which corresponds to an 80% increase in β from $I =$ 0.01 M to $I = 0.1$ M NaBr. Comparison of 0.05 M and 0.1 M NaBr slopes were not significantly different (Table 3, Figure 6B).

Figure 6C shows the quantitative data for the ⟨120⟩ step velocity measurements as a function of barium activity at the three different $NaNO_3$ ionic strengths. Comparing the kinetic coefficients of the different ionic strengths of the $NaNO_3$ solutions (Table 2), there is strong evidence that there is a significant difference in the kinetic coefficient between 0.01 M and 0.05 M $NaNO_3$. There is also strong evidence that there is a statistical difference between the kinetic coefficient of 0.01 M and 0.1 M $NaNO_3$ (Figure 6A, Table 3). The estimate for the difference in slope from these two solutions is 0.22 cm/s, which corresponds to a 130% increase in β from I = 0.01 M to I = 0.1 M $NaNO_3$. To summarize the kinetic coefficient results thus far, I does appear to positively influence β in each of the different salt solutions, but the quantitative effect corresponds to a moderate increase in β of 55-130% resulting from an order of magnitude increase in I.

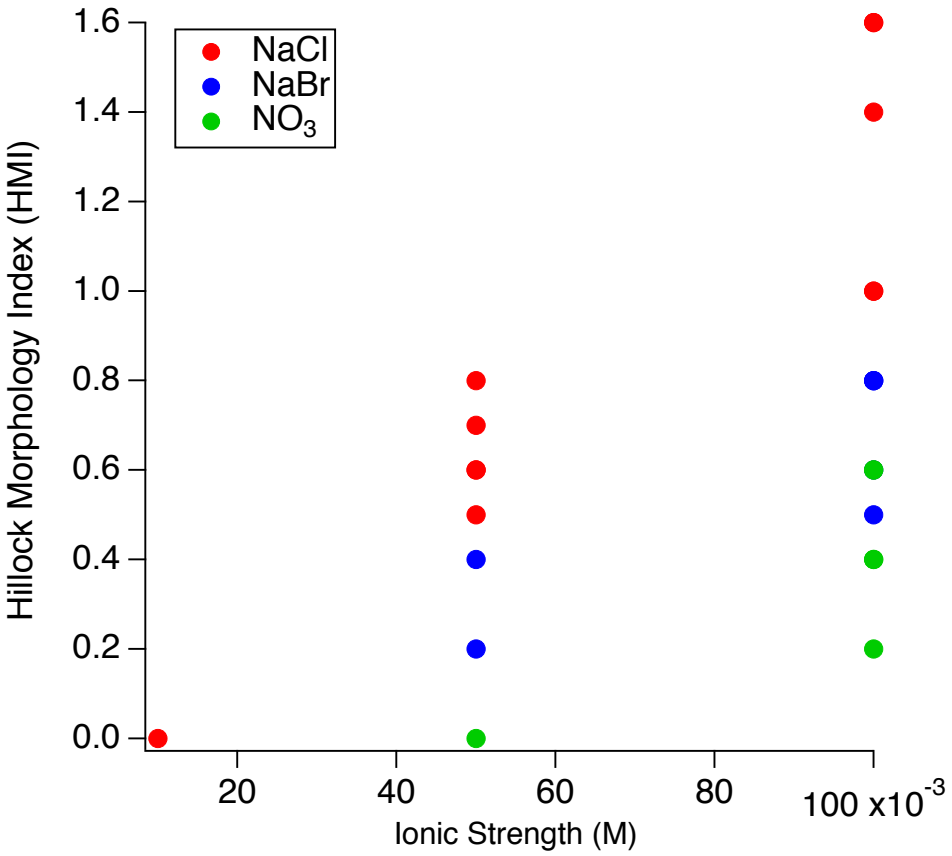

Figure 5: Hillock Morphology Index (HMI) number versus ionic strength (M) for solutions that show the presence of [010]. At 0.01 M, all salts have an HMI of 0.

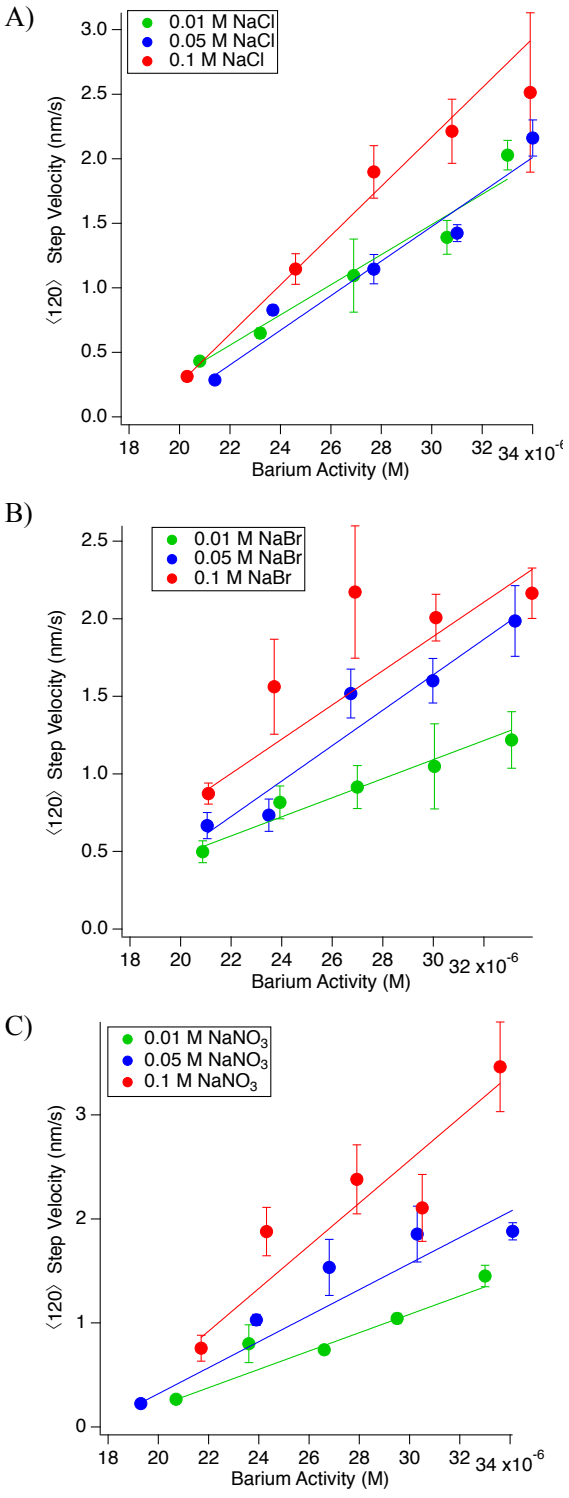

Figure 6: ⟨120⟩ step velocity (nm/s) versus barium activity (M) for 0.01, 0.05, and 0.1 M NaCl solutions (A, B and C, respectively) and respective model fits. Kinetic coefficients were derived from the slope of the linear fitting functions.

Table 2: Step kinetic coefficients for NaCl, NaBr and $NaNO_3$ at each ionic strength. Uncertainties in the least significant digit are indicated in parentheses.

Ionic Strength (M)	β_{NaCl} (cm/s)	β_{NaBr} (cm/s)	β_{NaNO_3} (cm/s)	a_{eq}(M) NaCl	a_{eq}(M) NaBr	a_{eq}(M) $NaNO_3$
0.01	$2.2(3) \times 10^{-1}$	$1.2(6) \times 10^{-1}$	$1.7(2) \times 10^{-1}$	$1.72(9) \times 10^{-5}$	$1.2(6) \times 10^{-5}$	$1.77(8) \times 10^{-5}$
0.05	$2.6(3) \times 10^{-1}$	$2.2(6) \times 10^{-1}$	$2.4(2) \times 10^{-1}$	$1.90(5) \times 10^{-5}$	$1.6(3) \times 10^{-5}$	$1.74(3) \times 10^{-5}$
0.1	$3.7(7) \times 10^{-1}$	$2.1(5) \times 10^{-1}$	$4(1) \times 10^{-1}$	$1.86(6) \times 10^{-5}$	$1.3(3) \times 10^{-5}$	$1.8(2) \times 10^{-5}$

Table 3: Statistical comparisons of kinetic coefficients, β (cm/s) between ionic strengths of salts and comparison between different salts at three ionic strengths ($\alpha = 0.1$). The p values that are significant are in bold.

Comparison of β: Ionic Strengths of Salts	***p* (NaCl)**	***p* (NaBr)**	***p* ($NaNO_3$)**
0.01 M vs 0.05 M	0.4065	**0.0465**	**0.0293**
0.01 M vs 0.1 M	**0.0831**	**0.0426**	**0.0745**
0.05 M vs 0.1 M	0.1623	0.8752	0.2046
Comparison of β: Salts at Ionic strengths	***p* (0.01 M)**	***p* (0.05 M)**	***p* (0.1 M)**
NaCl vs NaBr	**0.0205**	0.6218	**0.0085**
NaCl vs $NaNO_3$	**0.0519**	0.6955	0.7344
NaBr vs $NaNO_3$	0.1036	0.7708	0.2984

Figure 7 shows the relationship between the kinetic coefficients and ionic strength for ⟨120⟩ steps for the different background electrolytes. The data in this figure graphically demonstrate that there is an increase in kinetic coefficient with an increase in ionic strength. In addition, there are statistical differences in kinetic coefficients between the salts at low ionic strength (Figure 7, Table 2), however at 0.1 M ionic strength there is a significant statistical difference between NaBr and NaCl kinetic coefficients. This statistical difference at higher I may be due to discordance in the two highest supersaturated solutions in 0.1 M NaBr data (Figure 6B). These two data points have lower step velocities than expected for the supersaturation at this ionic strength and so this may result in the statistical difference.

There may be a modest difference between anions only at low ionic strength and at higher ionic strengths there is no major influence of type of anion on the step velocities (Figure 8) which is supported in comparing the kinetic coefficients of the different background electrolytes at the same ionic strength (Table 2). There is strong evidence to suggest there is a significant difference in kinetic coefficients between 0.01 M NaCl and NaBr. The estimate for this difference was 0.11 cm/s, corresponding to a kinetic coefficient in NaCl that is 83% greater than the respective coefficient in NaBr at $I = 0.01$ M. There is furthermore strong evidence to suggest that there is a significant difference between the kinetic coefficients of NaCl and $NaNO_3$ at $I = 0.01$ M. The estimate for the difference in the kinetic coefficient is 0.055 cm/s, corresponding to a kinetic coefficient in NaCl that is 29% greater than the respective coefficient in $NaNO_3$ at $I = 0.01$ M. All other comparisons to $NaNO_3$ solutions produced statistical results that were insufficient to support any conclusion of differences compared to NaCl or NaBr. From the analysis of comparing the kinetic coefficients of 0.05 M salts, there are no statistically significant

differences between the kinetic coefficients of the salts. There is, however, strong evidence to suggest that there is a significant difference in kinetic coefficients between 0.1 M NaCl and 0.1 M NaBr. However, examining Figure 7, shows that for NaCl and $NaNO_3$, there is an increase in kinetic coefficient with an increase in *I*, but for NaBr the kinetic coefficient decreased at high *I* which is discordant with the general trend. The kinetic coefficient for 0.1 M NaBr is not in line with the trend that NaCl and $NaNO_3$ follow resulting in the *p* value in Table 3 for 0.1 M NaCl versus NaBr being significant. The two highest supersaturation data points of 0.1 M NaBr found in Figure 8C are discordant with the trend that step velocities are higher at higher supersaturations. The two data points that are conflicting seem to plateau in step velocity instead of increasing with supersaturation. The estimate for the difference in kinetic coefficients is 0.15 cm/s, corresponding to a kinetic coefficient for NaCl that is 62% greater than the respective coefficient for NaBr. While there is a clear statistical difference between kinetic coefficients of NaCl and NaBr in 0.01 M and 0.1 M solutions, there may be a statistical difference at 0.05 M, however, due to the scatter in the data there is insufficient evidence to conclude that there is a likely statistical difference (Table 3).

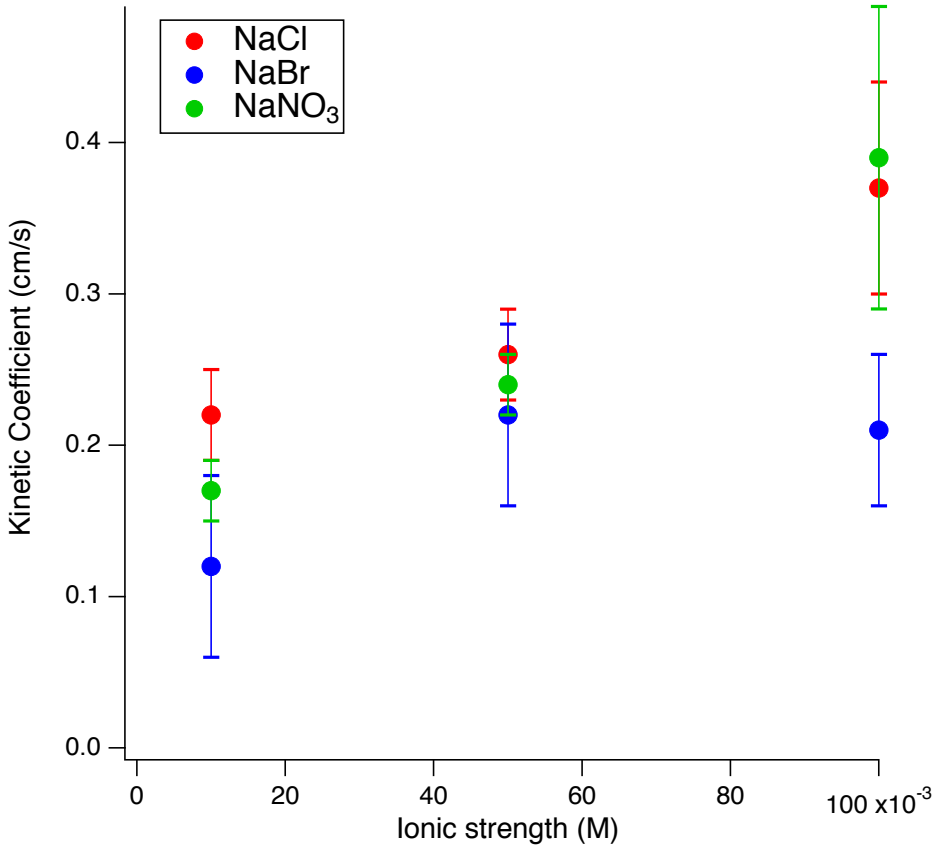

Figure 7: Kinetic coefficient (cm/s) for ⟨120⟩ steps versus ionic strength (M) for the three background electrolyte solutions.

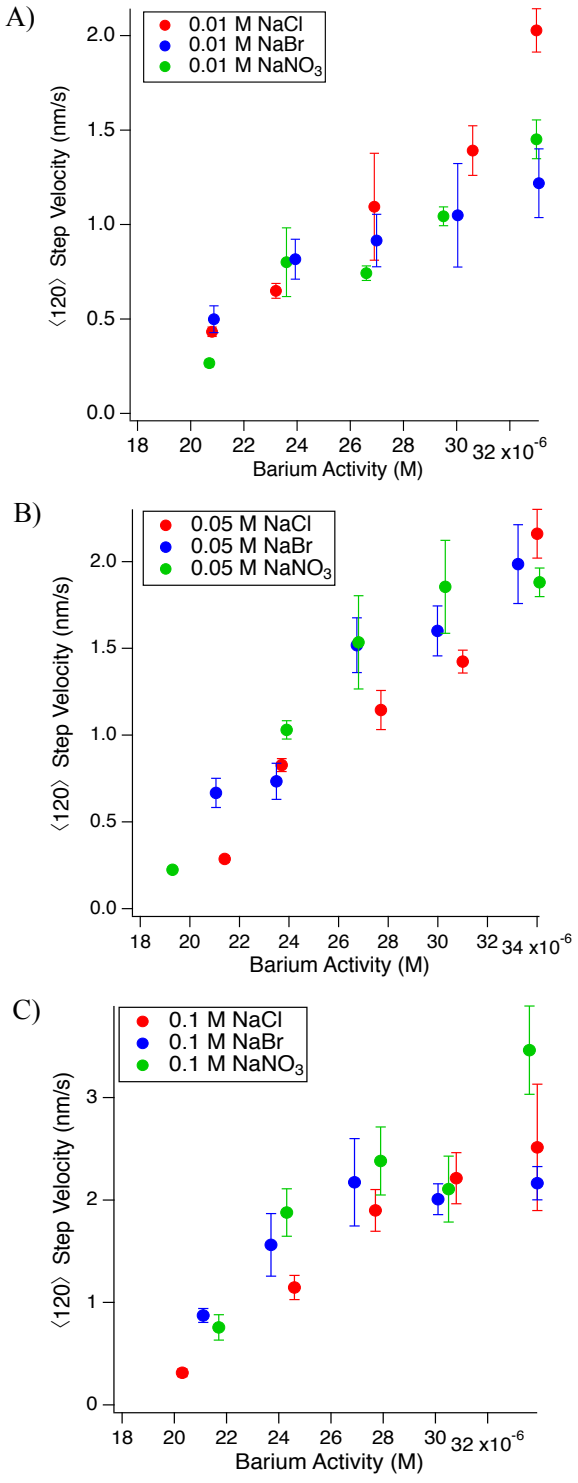

Figure 8: ⟨120⟩ step velocity (nm/s) versus barium activity (M) for NaCl, NaBr, and $NaNO_3$ at three *I* of 0.01 M, 0.05 M, and 0.1 M (A, B and C, respectively).

IV. DISCUSSION

Understanding the role of spectator ions on barite hillock growth is essential in recognizing key influences that affect growth kinetics. By studying solutions with different electrolytes, we have observed how the electrolyte anions and their concentrations influence hillock morphology and step growth velocities.

Hillock Morphology

In examining the influence of ions on hillock morphology it was found that with an increase of ionic strength, there is an increase in HMI for all the anions with HMI increasing in order of NO_3^-< Br^-< Cl^- (see Figures 2-4, Figure 5). The presence of [010] steps at higher ionic strength for all three background electrolytes may result in ion replacement reactions at the polar [010] steps resulting in electrostatic stabilization of these edges, consistent with previous hypotheses posed by Risthaus et al.[17] and Becker et al.[18] At higher ionic strengths, the background electrolyte is more effective at screening the polar fields on the [010] step, so that [010] step edge energy is reduced more significantly than the ⟨120⟩ steps.[18] Increasing HMI with *I* is also evident in $NaNO_3$, however the onset of [010] step appearance occurs only at the highest *I*. The presence of [010] steps with NaCl and NaBr solutions but the absence of [010] steps at lower *I* of $NaNO_3$ solutions suggest that there may be some interaction of the anion, particularly Cl^- and Br^-, with the [010] steps, which is in contrast to the presumption that Na^+ primarily interacts with [010] steps (Figure 5).[18] The electrolytes can affect the activities of barium and sulfate in solution, thereby affecting solubility of barium sulfate which is known to be an inverse function of

interfacial energy.[17,20] The electrolyte solutions increase the solubility of barite and therefore decrease the interfacial tension between solution and the crystal and the different background electrolytes change the interfacial tension differently.[20] The presence or absence of the [010] step at specific ionic strengths and the differences of HMI among the electrolytes suggest that different anions could change the barite-water interfacial energy by differing amounts, particularly through the stabilization of certain steps and/or crystal facets.

It is evident in the hillock morphology data in Figures 2-4 that the type of anion in the background electrolyte influences the onset of [010] steps. Hillocks formed in the presence of the chloride anion have higher HMI (i.e., prevalence of [010]) than the HMI of those formed in nitrate or bromide solutions. These differences in HMI demonstrate that the anion plays a role in barite growth. One possible explanation for the presence of the [010] steps in higher *I* solutions is that the anions will contribute to how water is structured around the barium cation and how effectively the [010] local electric field is screened.[17,19] Kowacz and Putnis,[19] found that with increasing *I* in the background electrolytes studied, islands and etch pits on barite during growth and dissolution, respectively, became elongated in the [010] direction, just as Risthaus et al.[17] found that hillocks became more elongated in the same direction with more sodium chloride. Another possible explanation of the differences in HMI between the anions is found in the details of the rate limiting mechanism of barite growth as discussed below.

Becker et al.[18] found that the rate-limiting step in barite growth was the formation of a new row along a kink-free step edge. From calculations in Becker et al.[18], the sodium ion adsorbing to the surface requires less energy than the barium ion attaching to the crystal

surface.[18] The weak and temporary adsorption of background electrolyte ions (*e.g.*, Na^+ or Cl^-) allows the subsequent substitution of barium or sulfate to be more energetically favorable than barium or sulfate ion to attach to "clean" sites.[18] Thus, the background electrolyte serves somewhat as a pre-cursor to the attachment of the crystal-building ions.

If we consider the temporary adsorption of Na^+ or respective anion (Cl^-, Br^-, NO_3^-) to a kink to form an ion pair with Ba^{2+} or SO_4^{2-}, then the differences in hillock morphology and corresponding kinetic coefficients may be linked to the kosmotropic/chaotropic character of the ions in solution. Kosmotropes, as explained by Collins,[27] are smaller ions that have a high charge density and are able to strongly bind to water more so than water interacts with itself, while chaotropes are larger ions that have low charge density and interact with water less than water binds with itself.[27] With kosmotropes, the water becomes less mobile than the bulk water and water in the presence of chaotropes is more mobile than the bulk.[27] Relative degrees of kosmotropic and chaotropic character of ions are based on the Jones-Dole viscosity *B* coefficient of the ions at room temperature[27] and there is some research into how temperature affects the coefficient[28] but the research field into inorganic salts is scarce. The kosmotropes in the solutions used in the experiments are Na^+, Ba^{2+}, and SO_4^{2-} where $Na^+ < SO_4^{2-} < Ba^{2+}$ in terms of the relative degrees of kosmotropic character with Jones-Dole viscosity *B* coefficients of 0.086, 0.208 and 0.22, respectively. The background anions studied are all classified as chaotropes with $Cl^- < Br^- < NO_3^-$ with Jones-Dole viscosity *B* coefficients of -0.007, -0.032 and -0.046, respectively. Na^+ is marginally kosmotropic and Cl^- is considered to be marginally chaotropic.[27] Br^- and NO_3^- are more chaotropic than Cl^- and therefore these two ions may hinder the breaking of the water shell around Ba^{2+} so that the sulfate ion can attach to kink sites.

The relative chaotropic nature of the anions may help explain why hillocks under Cl^- had the greatest HMI at high ionic strength followed by $Br^- > NO_3^-$ (Figure 5). In general, the strongest interactions in ionic solutions are kosmotropes interacting with other kosmotropes, then kosmotrope-water interactions, then water–water interactions, followed by chaotrope-water interactions and finally the weakest interaction is chaotropes with other chaotropes.[27] Therefore, the strongest ion pair interactions involving the barite/solution interface are Na^+-SO_4^{2-}, Ba^{2+}-Cl^- >> Ba^{2+}-Br^- > Ba^{2+}-NO_3^-. Although the temporary adsorption of spectator ions to the barite steps represents weak interactions, the strongest interactions can help to catalyze barium or sulfate attachment to the steps. The marginal chaotropic character of Cl^- may form a stronger interaction with a step (both [010] step and ⟨120⟩ steps) than the other anions, thereby allowing the [010] step to become more stable (i.e., higher HMI) at lower ionic strengths (Figure 5). The HMI increased in order of NO_3^- < Br^- < Cl^- and chaotropic character increases in order the opposite order of Cl^- < Br^- < NO_3^- suggesting that the presence of the [010] step is influenced by the ability of barium and sulfate to shed water or by temporary ion adsorption to steps in which strong interactions help growth.

Another explanation for the trend in HMI increasing in order of NO_3^- < Br^- < Cl^- involves the consideration of the sizes of the ions. The size of the anion may play a role in the ion's interactions with the [010] step. The sizes of the anions increase in order of Cl^- < Br^- < NO_3^-, with reported thermochemical radii as 0.168, 0.190 and 0.200 nm, respectively.[29] Specifically, in examining the HMI of NO_3^- versus Cl^-, the HMI of NO_3^- at higher *I* is less than or equal to the HMI of Cl^- at lower *I*. This suggests that NO_3^- interacts weakly, relative to Cl^-, with the [010] step which could be due to the ionic size. One

possible physical role played by ion size may be the steric hindrance towards anion attachment to the step with larger anions, such as nitrate, being more easily blocked or hindered by the surrounding step structure.

Examination of how the presence of different anions influences hillock morphology showed that under chloride, the [010] steps become stabilized and more prevalent under both *I* of 0.05 M and 0.1 M whereas under Br^- and NO_3^-, the [010] steps were established under higher *I*. Although we studied the effect of spectator anions on barite growth, the presence of the sodium ion is also important in catalyzing the attachment of the barium ion to a step.[17,18] Both the cation and anion of the background electrolyte are able to influence barite growth by how they structure water, stabilize local electric fields, and allow temporary adsorption to a site for rapid crystal unit attachment.

In summary, the background electrolyte and its concentration have been found to affect the barite hillock morphology. Under all three spectator ions, the HMI > 0 at high ionic strength, while hillocks formed under Cl^- had HMI > 0 for *I* of 0.05 M. The HMI at *I* = 0.1 M followed the order: $Cl^- > Br^- > NO_3^-$, suggesting that the spectator ion plays a role is stabilizing the [010] step direction.

Kinetic Coefficient

In investigating the ⟨120⟩ step velocities, there is evidence to indicate an increase in kinetic coefficient with an increase in ionic strength for each salt (Table 2), in agreement with the observations of Risthaus et al.,[17] Kowacz and Putnis,[19] and He et al.[20] However, these increases in β are small, requiring statistical analysis to detect the probable differences, and not as large, on a percentage basis, in comparison to previous studies.[17,19] Kowacz and Putnis[19] reported that island spreading velocity increased over 200% with an

increase in I from 0.01 M NaCl to 0.1 M NaCl, while the kinetic coefficients in NaCl only increased by 55% as reported here. Specifically, in investigating the salts at high ionic strength there may be a deviation from linearity at high barium activity (Figure 7C). This sub-linearity could be attributed to impurities,[9] however, reagents used in these studies are high purity trace metal grade reagents. These sub-linearities could be due to solution stability issues (see Appendix B) so that at higher barium activities, the step velocities represent velocities found at lower saturations. The lower step velocities at higher barium activity due to instability results in an underestimation of the kinetic coefficients at higher ionic strengths, which could lead to only modest differences in kinetic coefficients. Another explanation for smaller differences in β compared to previous studies is that Kowacz et al.[19] studied barite island growth under ambient temperatures while the current barite hillock growth studies were at higher temperature where it is possible that the ionic strength dependence of the kinetic coefficient is lessened. The measurements of Kowacz and Putnis[19] were also fundamentally different (i.e., island spreading velocities) from the current work (i.e., elementary step velocities) and therefore direct comparison of these studies is probably not appropriate.

In general, with an increase in ionic strength, there is a decrease in interfacial energy (or step edge Gibbs energy) between the crystal and solution as described by He et al.[20], who quantified interfacial energy of barite-water interfaces using nucleation studies. The interfacial energy is comprised of the Gibbs energy associated with terraces, steps and associated adsorbates that define the barite-water interface and as such, a decrease in the interfacial energy may be due to a decrease in the step edge Gibbs energy. A decrease in the step edge Gibbs energy results in an increase in the kink density along a step, thereby

promoting growth of the crystal as the step velocity is the product of the kink density and kink propagation velocity.[8,17]

There is evidence of possible mechanisms for barium ion attachment to a ⟨120⟩ step where the spectator ions could aid in barite growth. Stack et al. conclude that the rate-limiting attachment step is the transition of an inner-sphere adsorbed Ba ion at the ⟨120⟩ step edge to a bidentate bound state.[30] Ionic strength and salt type could affect the activation energy and the addition of background electrolyte can aid barium attachment to kink sites.[30] The spectator ions may promote the rate-limiting transition of an inner sphere adsorbed Ba to a bidentate state by catalyzing the Ba ion attachment process by temporarily adsorbing to a step edge, or by direct interaction with the Ba ion, resulting in a decreased activation barrier associated with the inner sphere-to-bidentate transition state.

In comparing the kinetic coefficients among the salts at low I, there are moderate differences in β at these low ionic strengths, suggesting that the identity of the spectator anion may influence barite growth (Figure 7). There is a general trend of increasing β with increasing I as discussed above, however, more importantly, the data demonstrate the significant differences observed among the salts at low ionic strength (Table 2). Although there is a significant difference between chloride and bromide kinetic coefficients at high ionic strength, this may be due to the discordant Br^- data points at higher supersaturation (Table 2, Figure 6B, Figure 7). The kinetic coefficients for bromide are less than those of nitrate at all ionic strengths, however, these are within the uncertainties, so that nitrate and bromide coefficients may be similar. The chaotropic nature of bromide and nitrate ions, as quantified by their respective Jones-Dole B coefficients, are more similar[27] than those of

bromide and chloride and so the kinetic coefficients could reflect these similarities and differences. The chaotropic nature of bromide and nitrate ions, as quantified by their respective Jones-Dole B coefficients, are more similar[27] than those of bromide and chloride and so the kinetic coefficients could reflect these similarities and differences. The presence of the chloride ion at $I = 0.01$ M yields a higher β than both nitrate and bromide anions (Table 2, Figure 7). To better understand how chloride may differ in its influence on barite step growth when compared with bromide and nitrate, we return to the consideration of the ions' influences on neighboring water structure. The ⟨120⟩ step velocities are influenced by the background electrolyte's ability to affect the water structure around barium or sulfate, which is influenced by the chaotropic and kosmotropic nature of the electrolyte ions. There is an activation energy that is associated with breaking the water shell around the crystal building units and the spectator ions assist in this desolvation.[19] The chloride anion is only marginally chaotropic and has a stronger interaction than bromide or nitrate ion with the barium ion. This stronger interaction may help to disrupt the hydration sphere of barium and therefore decrease the activation energy of barium ion moving, for example, from inner-sphere adsorbed to bidentate coordination at a step as reported from simulations by Stack et al.[30] The increase in step velocities under the presence of chloride, even at low I, suggests that the chloride ion may be able to help facilitate the rate-limiting step in attaching the barium ion to a step site.[30]

The differences in kinetic coefficients at low ionic strength between the different anions are enhanced due to the relative lack of availability of spectator ions compared to the solutions of higher ionic strength. At low ionic strength, the kink population is relatively small compared to higher ionic strengths, so there is more competition for access to these

kinks. The advancement of barite steps at lower ionic strength is therefore hindered relative to advancement at higher ionic strengths. The ability of the different anions to interact with the surface and to structure water around barium ions will reflect the competition for kink sites and result in different growth rates. Specifically, barite growth is positively influenced under chloride at low ionic strengths, suggesting that the chloride ion is more capable of assisting barium attachment to kinks due to chloride's marginally chaotropic character. The stronger chaotropic nature of bromide and nitrate anions may hinder the anion's ability to assist barium ion to shed its water shell in order to attach to a kink leading to lower kinetic coefficients. Under higher ionic strengths, the interfacial energy is decreased,[18] resulting in a higher kink density along steps, reducing the aforementioned competition for attachment at these sites. In addition, the possible lowering of the activation barrier to Ba ion attachment by the electrolyte anion lessens the impedance to barite growth. If the spectator anion helps to lower the activation energy for Ba^{2+} attachment at the ⟨120⟩ steps, the addition of electrolytes at higher concentrations may result in the emergence of a different rate-determining step than the step at lower ionic strengths. This new rate-determining step may not involve the background electrolyte ion and so therefore may lead to similar kinetic coefficients at higher ionic strengths.

Increasing I by an order of magnitude (0.01 M to 0.1 M) for each background electrolyte lead to a modest increase in β by 55-130% (Table 2). This moderate increase in the kinetic coefficients for each anion demonstrates an influence of ionic strength on barite growth. Along with an increase in anion concentration with higher ionic strength there is also an increase in the amount of sodium ion available. For comparison, higher concentrations of the kosmotropic OH^- ion in a pH study conducted by Ruiz-Agudo et al.

showed an increase in barite growth possibly due to an increase in bulk water exchange with barium ion to help with desolvation at a barite surface.[12] The sodium ion also has kosmotropic characteristics in our solutions and the increase in the Na^+ concentrations may, in addition to the anion, display a positive effect on kinetic coefficient. Given the potential role of the spectator cation in barite growth, a systematic study of various electrolyte cations will be studied in future experiments.

V. CONCLUSION

The concentrations of the background electrolyte influence both barite hillock morphology as well as step velocities. The background electrolyte, as well as *I*, affects the prevalence of the [010] step direction with HMI increasing in order of NO_3^- < Br^- < Cl^-, demonstrating that the spectator anion may play a role in barium attachment mechanisms as well as decreasing the Gibbs energy of the unstable and polar [010] step. In general, with respect to kinetic coefficients, there is a modest increase in β with an increase in *I* for each salt within the uncertainties. The role of the spectator anion is highlighted in the differences in kinetic coefficients at low *I* with the possibility that the spectator anion identity may affect the activation energy of barium attachment differently due to how the anion is able to structure water around the barium cation.

Future Work:

While this study has investigated the role of the background electrolyte anions on barite growth, there are still unanswered questions that should be examined further. Investigation into the role of cation spectator ions on barite step edge growth kinetics should be performed in order to distinguish distinct roles that the cation may play on barite growth compared to the anion. The background electrolytes should contain a chloride anion and the cations should be from the alkali metals (Li, K, Rb and Cs). Solution compositions should be the same with *I* being 0.01 M, 0.05 M and 0.1 M as well as *SI* ranging from 0.1 to 0.5. Special attention should be given to how the background electrolytes and *I* affect hillock morphology and the onset of [010] step direction. HMI numbers should be assigned

to the hillocks under the different solutions in order to more quantitatively compare the hillocks formed under NaCl found in these experiments.

Investigation into which method of data acquisition and analysis (See Appendix B) may be required in order to address the large uncertainties in some of the velocity data. Future work into software development for HAFM images and step velocity analysis is recommended. Also it is recommended that there is more examination of the statistical analysis to determine the number of data points that would be required for an acceptable sample size for analysis.

The solution stability issue also should be investigated further. Another method, besides the HAFM should be utilized to monitor solution instability over time. The background electrolyte, ratio of barium to sulfate, saturation index as well as ionic strength may affect the solution instability (See Appendix B). Specifically, investigating solution stability at higher ionic strength as well as NaBr solutions in general is needed to clarify the data presented in this study. At high ionic strength, there may be sub-linearity resulting in an underestimation for the kinetic coefficients.

To identify if the rate-limiting step for barium attachment changes from lower ionic strength to higher ionic strength, more experiments should be performed at lower ionic strengths to ensure that there is a statistical difference in the data at low ionic strength. If there is indeed a statistical difference at low ionic strength, then a study on the effect of ionic strength on activation energies can be performed to determine if ionic strength has an effect on barium attachment activation energies.

REFERENCES:

1. Paytan, A.; Averyt, K.; Faul, K.; Gray, E.; Thomas, E. Barite accumulation, ocean productivity, and Sr/Ba in barite across the Paleocene-Eocene Thermal Maximum. *Geology* **2007***, 35*, 1139-1142.

2. Boerlage, S. F. E.; Kennedy, M. D.; Bremere, I.; Witkamp, G. J.; Van, d. H.; Schippers, J. C. The scaling potential of barium sulphate in reverse osmosis systems. *J. Membr. Sci.* **2002***, 197*, 251-268.

3. Curti, E.; Fujiwara, K.; Iijima, K.; Tits, J.; Cuesta, C.; Kitamura, A.; Glaus, M. A.; Mueller, W. Radium uptake during barite recrystallization at 23 +/- 2 degrees C as a function of solution composition: An experimental Ba-133 and Ra-226 tracer study. *Geochim. Cosmochim. Acta* **2010***, 74*, 3553-3570.

4. Ferrar, K. J.; Michanowicz, D. R.; Christen, C. L.; Mulcahy, N.; Malone, S. L.; Sharma, R. K. Assessment of Effluent Contaminants from Three Facilities Discharging Marcellus Shale Wastewater to Surface Waters in Pennsylvania. *Environ. Sci. Technol.* **2013***, 47*, 3472-3481.

5. Warner, N. R.; Christie, C. A.; Jackson, R. B.; Vengosh, A. Impacts of Shale Gas Wastewater Disposal on Water Quality in Western Pennsylvania. *Environ. Sci. Technol.* **2013***, 47*, 11849-11857.

6. Burton, W. K.; Cabrera, N.; Frank, F. C. The Growth of Crystals and the Equilibrium Structure of their Surfaces. *Philosophical Transactions of the Royal Society of London. Series A, Mathematical and Physical Sciences* **1951**, *243*, 299-358.

7. Chernov, A. A.; Rashkovich, L. N.; Yaminski, I.; Gvozdev, N. V. Kink kinetics, exchange fluxes, 1D 'nucleation' and adsorption on the (010) face of orthorhombic lysozyme crystals. *J. Phys.:Condens. Matter* **1999**, *11*, 9969-9984.

8. Frank, F. C. Nucleation-controlled growth on a one-dimensional growth of finite length. *J. Cryst. Growth* **1974**, *22*, 233-236.

9. Teng, H.; Dove, P.; DeYoreo, J. Reversed calcite morphologies induced by microscopic growth kinetics: Insight into biomineralization. *Geochim. Cosmochim. Acta* **1999**, *63*, 2507-2512.

10. Bracco, J. N.; Gooijer, Y.; Higgins, S. R. Hydrothermal atomic force microscopy observations of barite step growth rates as a function of the aqueous barium-to-sulfate ratio. *Geochim. Cosmochim. Acta* **2016**, *183*, 1-13.

11. Bracco, J. N.; Gooijer, Y.; Higgins, S. R. Growth kinetics of step edges on celestite (001) surfaces as a function of temperature, saturation state, ionic strength, and aqueous strontium: sulfate ratio: An in-situ atomic force microscopy study. *Geochim. Cosmochim. Acta* **2016**, *175*, 222-238.

12. Ruiz-Agudo, C.; Putnis, C. V.; Ruiz-Agudo, E.; Putnis, A. The influence of pH on barite nucleation and growth. *Chem. Geol.* **2015**, *391*, 7-18.

13. Pina, C.; Becker, U.; Risthaus, P.; Bosbach, D.; Putnis, A. Molecular-scale mechanisms of crystal growth in barite. *Nature* **1998**, *395*, 483-486.

14. de Antonio Gomez, S.; Pina, C. M.; Martin-Bragado, I. Lattice Kinetic Modeling of the Anisotropic Growth of Two-Dimensional Islands on Barite (001) Surface. *Cryst. Growth Des.* **2013**, *13*, 2840-2845.

15. Kuwahara, Y.; Liu, W.; Makio, M.; Otsuka, K. In Situ AFM Study of Crystal Growth on a Barite (001) Surface in BaSO4 Solutions at 30 degrees C. *Minerals* **2016**, *6*, UNSP 117.

16. Godinho, J.; Stack, A. G. Growth Kinetics and Morphology of Barite Crystals Derived from Face-Specific Growth Rates. *Cryst. Growth Des.* **2015**, *15*, 2064-2071.

17. Risthaus, P.; Bosbach, D.; Becker, U.; Putnis, A. Barite scale formation and dissolution at high ionic strength studied with atomic force microscopy. *Colloids Surf. Physicochem. Eng. Aspects* **2001**, *191*, 201-214.

18. Becker, U.; Risthaus, P.; Bosbach, D.; Putnis, A. Selective attachment of monovalent background electrolyte ions and growth inhibitors to polar steps on sulfates as studied by molecular simulations and AFM observations. *Mol. Simul.* **2002**, *28*, 607-632.

19. Kowacz, M.; Putnis, A. The effect of specific background electrolytes on water structure and solute hydration: Consequences for crystal dissolution and growth. *Geochim. Cosmochim. Acta* **2008**, *72*, 4476-4487.

20. He, S.; Oddo, J.; Tomson, M. The Nucleation Kinetics of Barium-Sulfate in Nacl Solutions Up to 6 M and 90-Degrees-C. *J. Colloid Interface Sci.* **1995**, *174*, 319-326.

21. Zhen-Wu, B. Y.; Dideriksen, K.; Olsson, J.; Raahauge, P. J.; Stipp, S. L. S.; Oelkers, E. H. Experimental determination of barite dissolution and precipitation rates as a function of temperature and aqueous fluid composition. *Geochim. Cosmochim. Acta* **2016**, *194*, 193-210.

22. Parkhurst, D. L.; Appelo, C. A. *Users Guide to PHREEQC (Version 2)- A Computer Program for Speciation, Batch Reaction, One Dimensional Transport, and Inverse Geochemical Calculations;* U.S Geological Survey: Denver CO, 1996; .

23. Helgeson, H. C. Thermodynamics of hydrothermal systems at elevated temperatures and pressures. *Am. J. Sci* **1969**, *267*, 729-804.

24. Higgins, S.; Eggleston, C.; Knauss, K.; Boro, C. A hydrothermal atomic force microscope for imaging in aqueous solution up to 150 degrees C. *Rev. Sci. Instrum.* **1998**, *69*, 2994-2998.

25. Land, T. A.; DeYoreo, J. J.; Lee, J. D. An in-situ AFM investigation of canavalin crystallization kinetics. *Surf. Sci.* **1997**, *384*, 136-155.

26. Becker, U.; Biswas, S.; Kendall, T.; Risthaus, P.; Putnis, C.; Pina, C. Interactions between mineral surfaces and dissolved species: From monovalent ions to complex organic molecules. *Am. J. Sci.* **2005**, *305*, 791-825.

27. Collins, K. D. Charge density-dependent strength of hydration and biological structure. *Biophysical Journal* **1997**, *72*, 65-76.

28. Abdulagatov, I. M.; Zeinalova, A.; Azizov, N. D. Viscosity of aqueous Na_2SO_4 solutions at temperatures from 298 to 573K and at pressures up to 40MPa. *Fluid Phase Equilib*. **2005**, *227*, 57-70.

29. Roobottom, H. K.; Jenkins, H. D. Thermochemical radii complex ions. *J. Chem. Educ.* **1999**, *76*, 1570.

30. Stack, A. G.; Raiteri, P.; Gale, J. D. Accurate Rates of the Complex Mechanisms for Growth and Dissolution of Minerals Using a Combination of Rare-Event Theories. *J. Am. Chem. Soc*. **2012**, *134*, 11-14.

APPENDIX A:

Crystal Growth:

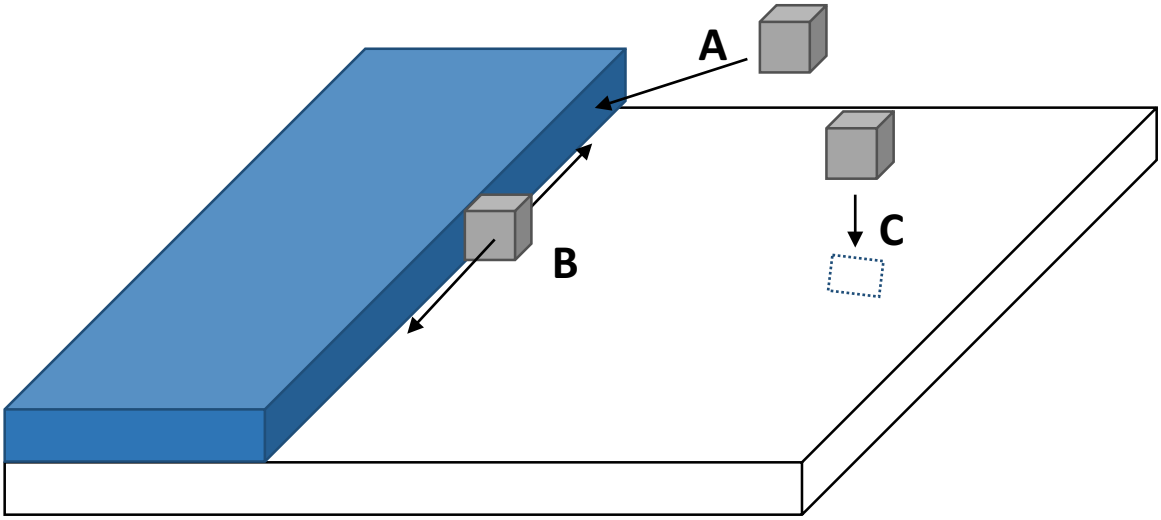

Figure A1:Example of crystal growth where A shows the attachment of a growth unit to a step edge, B shows a growth unit attached to the step edge and growth can occur laterally and C shows a growth unit adsorbing to the terrace (Illustration derived from [1,2])

The crystal-water interface is under constant fluctuations involving attachment and detachment of crystal units and each is an independent process with kinetic barriers and frequencies. When the rate of kink generation is comparable to the rate of kink propagation, the kink density will be large and there are many sites for attachment and detachment of the crystal units. [3] Figure A1 demonstrates different mechanisms of growth of a crystal where (A) shows a growth unit adsorbing to a step edge creating a kink site (B) that has attachment sites where the step can grow laterally with the addition of other growth units and (C) shows that a growth unit can adsorb to the terrace.[1]

Barite Crystallography:

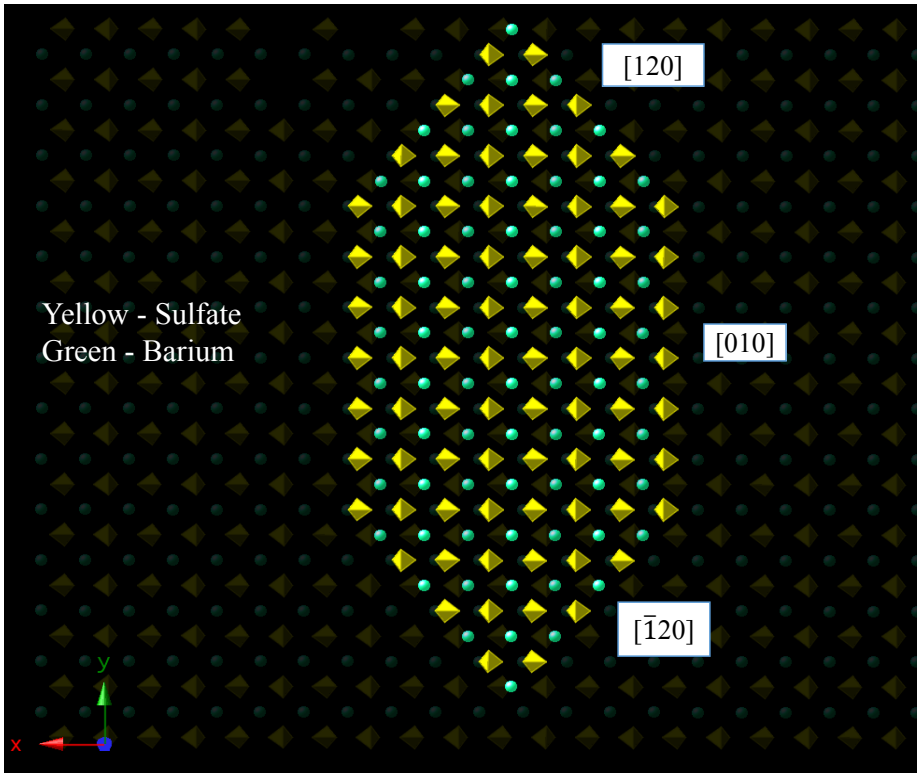

Figure A2: Structure of barite surface (001) with common step orientations of ⟨120⟩ and [010].

Barite ($BaSO_4$) is a AB mineral type with an orthorhombic lattice meaning that the perpendicular axes are different lengths; a = 8.87, b= 5.45 and c= 7.14 angstroms. [4] Figure A2 shows the structure of the barite (001) surface that is studied and the common step orientations. The ⟨120⟩ step orientation is terminated by alternating barium and sulfate ions, effectively making this step termination non-polar while the [010] step is terminated by either barium cations or sulfate anions and thus it is a polar step termination.[5]

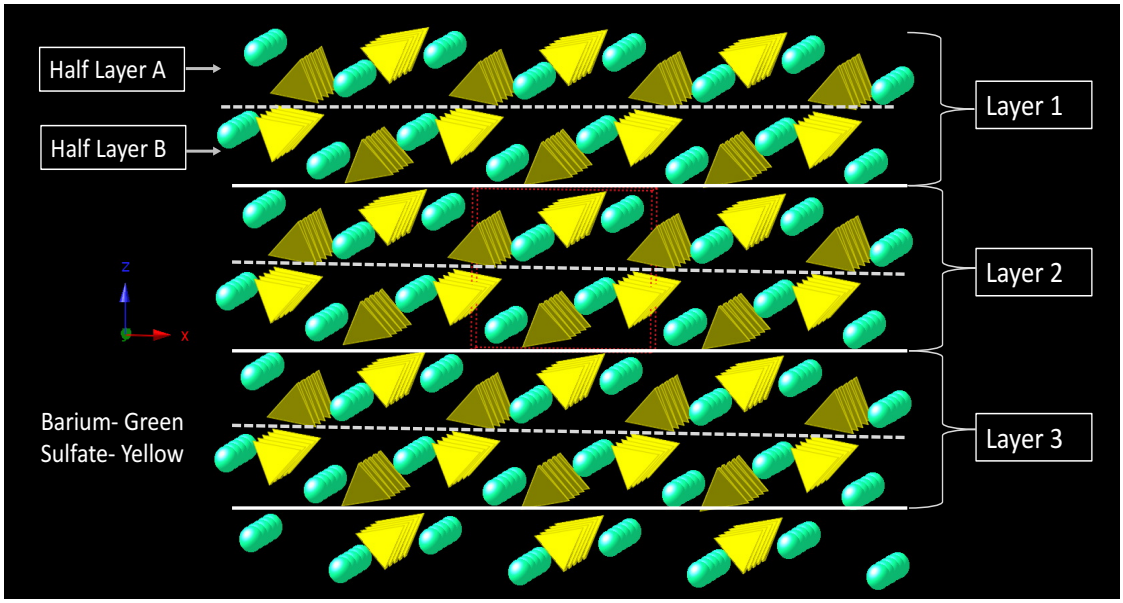

Figure A3: Side view of barite(001), made up of full layers and half layers. The half layers are related by a screw axis.

Perpendicular to the (001) face of barite, is made up of full and half layers, where the half layers are related by a 2^1 screw axis parallel to c axis (Figure A3). The 2 in the 2^1 screw axis means that the first half layer is rotated 180° (360/2) compared to the second half layer and then there is a half unit cell translation (1/2t). [4] This results in the barite growth hillocks consisting of both half layer (3.57 angstroms) and full layers (7.14 angstroms). [6]

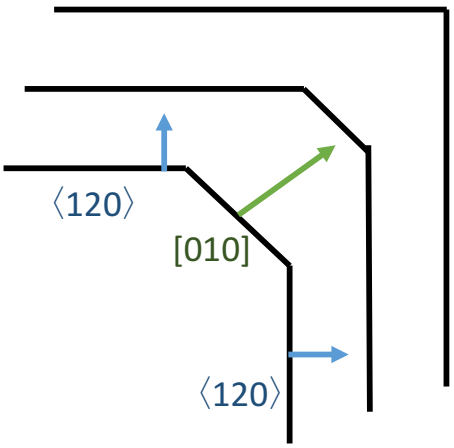

Figure A4: Demonstration of barite hillock growth in which the [010] step direction grows much faster than the ⟨120⟩ step direction so that the hillock only contains the slower growing step direction.

Figure A4 shows that if [010] step growth velocities are much greater than ⟨120⟩ step growth velocities then the hillock will only show the presence of ⟨120⟩ steps, due to the ⟨120⟩ step being the slowest growing step direction. Due to the absence of [010] steps in most of the hillocks under the conditions that we have examined, we collect step velocities of the ⟨120⟩ steps.

Hydrothermal Atomic Force Microscope:

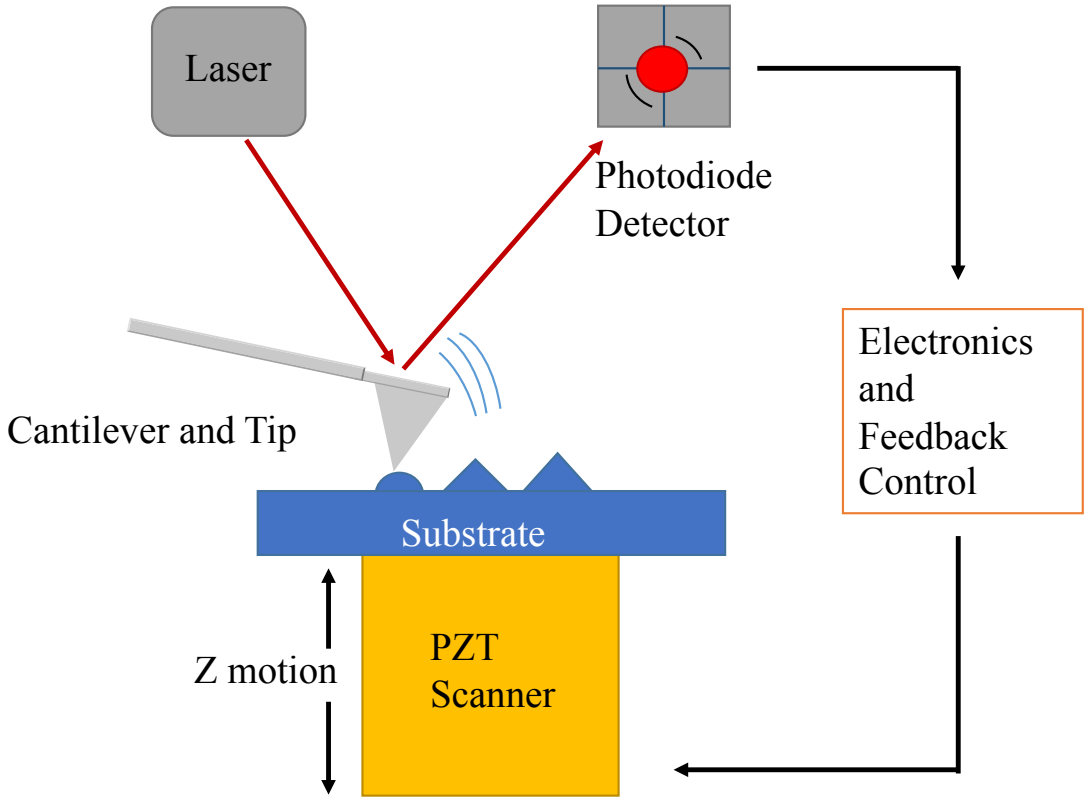

Figure A5: Schematic derived from Bracco[7] and Reifenberger [8] showing how the cantilever's deflection, which is effected by the topography of the sample surface, is monitored by a laser and photodiode detector, which is connected to the electronic system and under feedback control which in turn moves the PZT (Lead Zirconate Titanate) Scanner.

The Atomic Force Microscope (AFM) is able to change the position of the sample under the cantilever using a piezoelectric scanner for atomic-scale control in conjunction with an optoelectronic system for detecting the deflection of the cantilever and feedback electronics for control of the force acting between the sharp tip on the end of the cantilever and the sample of interest. In order to study surface morphology and growth at AFM is used to study surface morphology at nm-μm scales, a piezoelectric scanner is used to move the sample under the cantilever tip. The piezoelectric material that produces a voltage when

a force is applied in a direction and AFM uses inverse piezoelectric effect in which minute (nm-μm) displacement in a certain direction occurs under voltage. [8] Lead Ziroconate Titanate (PZT) material is used as the piezoelectric material in Figure A5. In contact mode, the goal of the AFM is to maintain a certain force between the tip and the sample. Figure A5 shows a cantilever and tip (triangle) close to the sample and a laser reflects off the back of the cantilever and is monitored by a four quadrant photodiode, which produces a set of voltage signals that are proportional to the intensity of light striking each detector. Subtle changes in the cantilevers deflection in real time will change the relative detector voltages which will be compared to a setpoint. The feedback control will work to move the PZT scanner so that the cantilever deflection is constant. The differences between the reference voltage and the voltage from the cantilever deflection gives an error signal which makes up the AFM deflection images. [8]

Hydrothermal Atomic Force Microscopy (HAFM) is an unique tool to study mineral surfaces, specifically minerals that grow too slow at room temperature and near equilibrium for AFM to monitor effectively. The HAFM allows surfaces to be monitored up to 150 ºC and under 6 atm pressure[9]and this allows sparingly-soluble minerals, such as barite, to grow with step velocities in the range of 0.1-10 nm/s under near equilibrium solutions. The HAFM also allows samples to be monitored *in-situ* using a wall-jet flow system, as described in Yamada and Matsuda (1973), [10] which introduces the solutions in such a way as to rapidly replace solution near the tip-sample contact and with well-defined hydrodynamics that have analytical solution. A flow rate controller is also used to set and monitor the flow rate at sufficiently high values so that the system growth kinetics are

independent of mass transport, leading to surface reactions to be associated with the rate-limiting step.

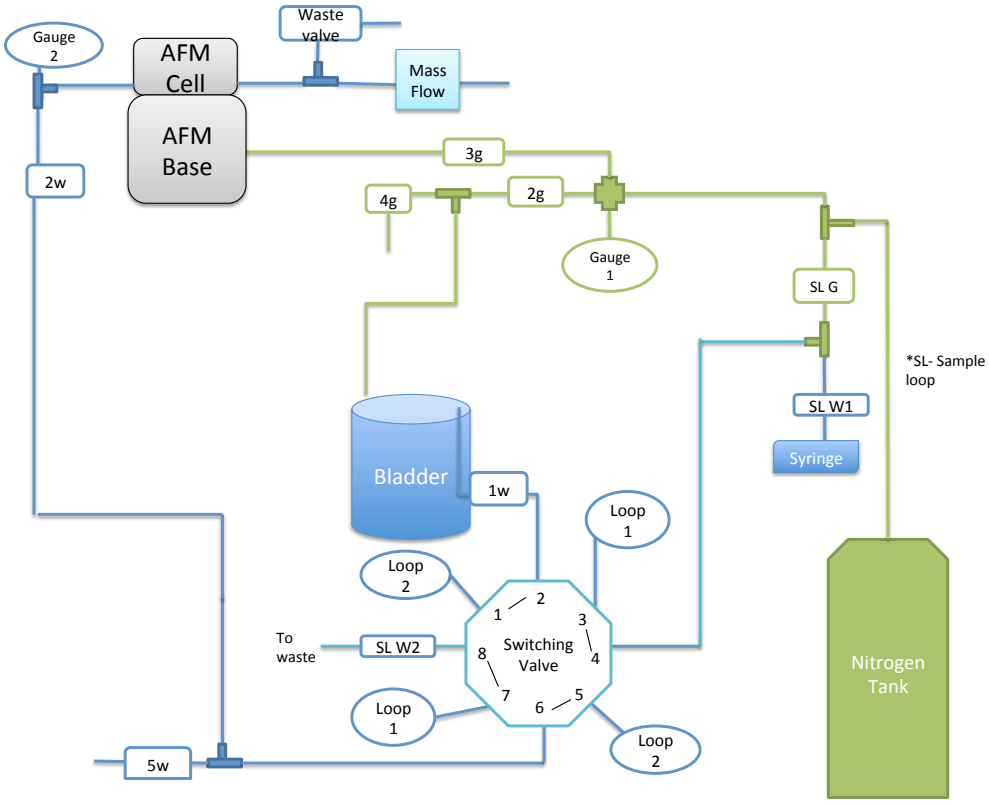

Figure A6: Schematic of HAFM set up where (g) represents valves that control the flow of nitrogen gas and (w) are valves that control the flow of liquid throughout the system.

Figure A6 shows a schematic of the plumbing that controls gas and liquid flow into the HAFM. The nitrogen is connected to Gauge 1, which measures the gas pressure. 2g allows gas to pressurize bladder and 3g allows the HAFM base to be pressurized while 4g is used to leak the gas to depressurize the system. SL G valve allows the sample loops (Loop 1 and 2) to be pressurized in order to switch solutions into the AFM cell under pressure during experiments. SL W1 is a switch valve that allows liquid from a syringe to fill a loop, while Loop 1 or 2 contains the liquid and SL W2 valve is a leak valve used

when filling loops with solutions. 1w switch valve allows water from the bladder to push and fill a loop with water. The loop that is in line with 1w is the loop that is connected to the AFM cell. 5w is another leak valve that is used if the solution entering the fluid cell has an air bubble. 2w allows fluid to enter the HAFM fluid cell and the pressure of the liquid is monitored by Gauge 2. There is another waste valve after the fluid enters and exits the HAFM fluid cell and the flow rate of the solutions are controlled by a mass flow controller that empties into waste.

Land et al.,[11] Method

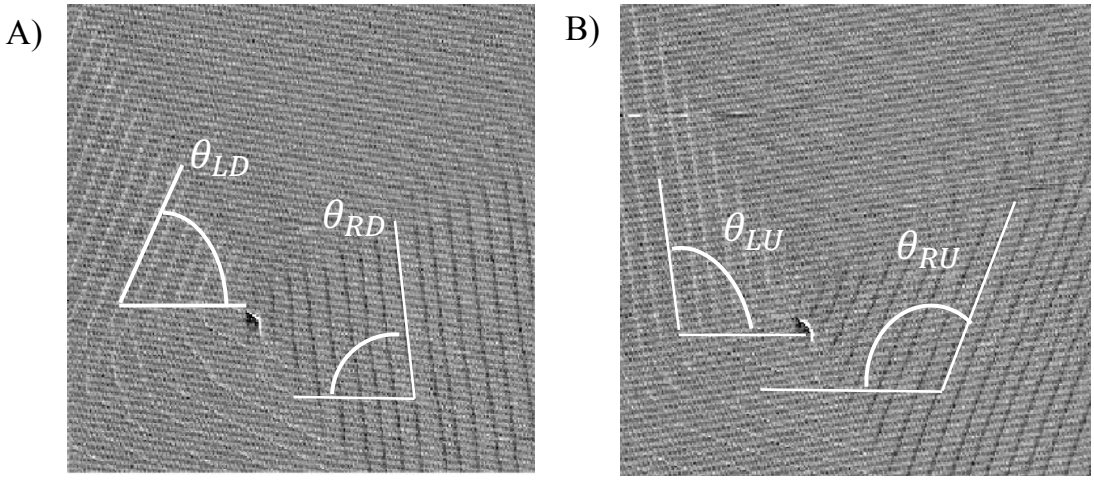

Figure A7: In-situ HAFM error signal images (giving appearance of illumination on the left) where A) is a down scan image and B) is an up scan. Examples of where angle measures used in Land's method are labeled on the images.

A) 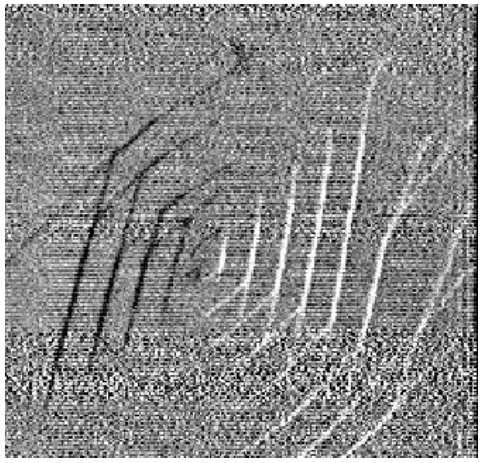 B) 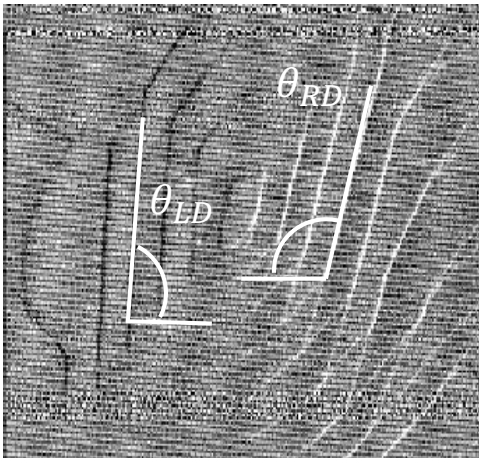

Figure A8:In-situ HAFM error signal images (giving appearance of illumination on the right) where A) is fast scan rate image (5 Hz) of hillock in B) which is a down scan image of a hillock taken at a slower scan rate of 2 Hz. The angle measurements for Land's method are labeled in B. [11]

Figure A7 demonstrates some considerations that need to be taken while experimenting and using Land's Method for data analysis. Land et al. report uncertainties up to 20% using this method. [11] However, these higher errors can be avoided by scanning slower during an experiment in order to have large differences in angles between up and down images as shown in Figure A7 and Figure A8.

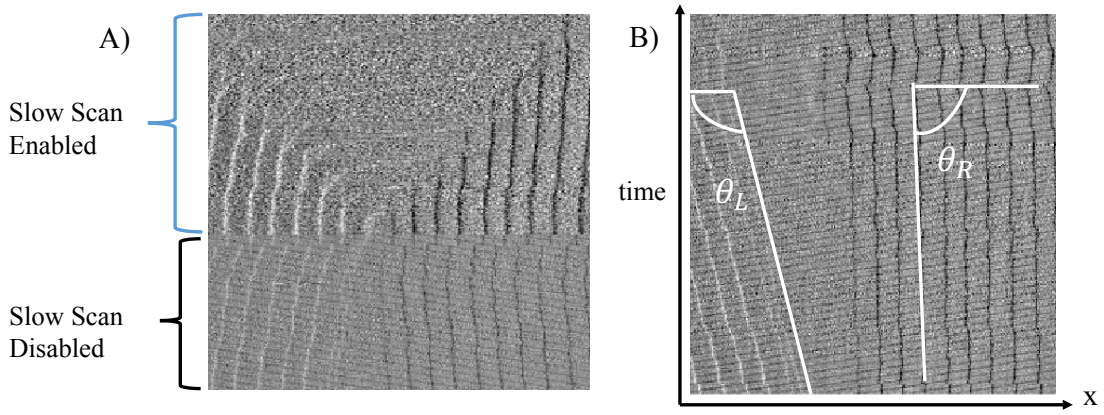

Figure A9: In-situ HAFM error signal images (giving appearance of illumination on the left) where A) demonstrates an image where the slow scan is enabled in the top half of the image and the slow scan is disabled in the bottom half. B) shows a full image of the slow scan disabled and angle measures collected using Teng's method are labeled. [12] B) demonstrates that an error signal image collected while the slow scan is disabled results in a time vs position graph essentially.

Another method for data analysis that is useful but more challenging to implement during experiments is the Teng method. [12] During experiments, the slow scan axis needs to be disabled as described in Figure A9. While this method only requires one image to be analyzed, obtaining an image for this method is challenging. Often during experiments, there is some thermal drift (the scanned area moves) so it is often useful to find a void or a defect that can be monitored while the slow scan is disabled. Another issue with disabling the slow scan is that the sample is more susceptible to tip wear [13] since there is only one line that is continually being scanned. Tip wear can be combated by decreasing the force used by the cantilever while scanning the surface.

APPENDIX A: REFERENCES

1. Burton, W. K.; Cabrera, N.; Frank, F. C. The Growth of Crystals and the Equilibrium Structure of their Surfaces. *Philosophical Transactions of the Royal Society of London. Series A, Mathematical and Physical Sciences* **1951**, *243*, 299-358.

2. Higgins, S.; Bosbach, D.; Eggleston, C.; Knauss, K. Kink dynamics and step growth on barium sulfate (001): A hydrothermal scanning probe microscopy study. *J Phys Chem B* **2000**, *104*, 6978-6982.

3. De Yoreo, J. J.; Zepeda-Ruiz, L. A.; Friddle, R. W.; Qiu, S. R.; Wasylenki, L. E.; Chernov, A. A.; Gilmer, G. H.; Dove, P. M. Rethinking Classical Crystal Growth Models through Molecular Scale Insights: Consequences of Kink-Limited Kinetics. *Cryst. Growth Des.* **2009**, *9*, 5135-5144.

4. Klein, C.; Hurlbut, C. S. J. *Manual of Mineralogy;* John Wiley & Sons, Inc.: New York, 1993; Vol. 21.

5. Becker, U.; Risthaus, P.; Bosbach, D.; Putnis, A. Selective attachment of monovalent background electrolyte ions and growth inhibitors to polar steps on sulfates as studied by molecular simulations and AFM observations. *Mol. Simul.* **2002**, *28*, 607-632.

6. Pina, C. M.; Bosbach, D.; Prieto, M.; Putnis, A. Microtopography of the barite (0 0 1) face during growth: AFM observations and PBC theory. *J. Cryst. Growth* **1998**, *187*, 119-125.

7. Bracco, J. N. Growth of Sparingly-Soluble AB-Type Minerals as a Function of their A:B ratio, Wright State University, 2015.

8. Reifenberger, Ronald G., *Fundamentals of Atomic Force Microscopy Part I: Foundations*. World Scientific: New Jersey, 2016; Vol. 4

9. Higgins, S.; Eggleston, C.; Knauss, K.; Boro, C. A hydrothermal atomic force microscope for imaging in aqueous solution up to 150 degrees C. *Rev. Sci. Instrum.* **1998**, *69*, 2994-2998.

10. Yamada, J.; Matsuda, H. Limiting diffusion currents in hydrodynamic voltammetry. III. Wall jet electrodes. *J Electroanal Chem* **1973**, *44*, 189-198.

11. Land, T. A.; DeYoreo, J. J.; Lee, J. D. An in-situ AFM investigation of canavalin crystallization kinetics. *Surf. Sci.* **1997**, *384*, 136-155.

12. Teng, H.; Dove, P.; De Yoreo, J. Kinetics of calcite growth: Surface processes and relationships to macroscopic rate laws. *Geochim. Cosmochim. Acta* **2000**, *64*, 2255-2266.

13. Park, N.; Kim, M.; Langford, S. C.; Dickinson, J. T. Atomic layer wear of single-crystal calcite in aqueous solution using scanning force microscopy. *J. Appl. Phys.* **1996**, *80*, 2680.

APPENDIX B:

Propagation of error

Propagation of error to obtain the standard deviation of the average step velocity is given by the following equations:

$$\sigma_{vs} = \frac{\sqrt{(\sigma_L)^2+(\sigma_R)^2}}{2} \tag{S1}$$

where the uncertainty in the step velocity of steps on one side of the hillock is approximated by:

$$\delta v = \sqrt{\left(\frac{\partial v}{\partial \theta_D}\delta\theta_D\right)^2 + \left(\frac{\partial v}{\partial \theta_U}\delta\theta_U\right)^2} \tag{S2}$$

$$\sigma_{LD\ or\ RD} = \frac{2RS\left(2+cot\theta_D cot\theta_u + cot\theta_u{}^2\right)csc\theta_D{}^2}{N(cot\theta_D+cot\theta_u)*(4+cot\theta_D{}^2+2cot\theta_D cot\theta_u+cot\theta_u{}^2)\sqrt{1+\frac{4}{(cot\theta_D+cot\theta_u)^2}}} \tag{S3}$$

$$\sigma_{Lu\ or\ Ru} = \frac{2RS\left(2+cot\theta_D{}^2+cot\theta_D cot\theta_u\right)csc\theta_u{}^2}{N(cot\theta_D+cot\theta_u)*(4+cot\theta_D{}^2+2cot\theta_D cot\theta_u+cot\theta_u{}^2)\sqrt{1+\frac{4}{(cot\theta_D+cot\theta_u)^2}}} \tag{S4}$$

where σ_{LD} is the standard deviation of the left side of the hillock angles during a down scan, R is the rate of which a scan of the image is taken (Hz), S is the scan area (nm), N is the number of lines in the image, θ_D is the average down scan angle, and θ_u is the average up scan angle. The average of the angles is taken from a group of angle measurements from each image. The error associated with the average step velocity is associated with the precision of the method of measuring angles.

Table S1: HMI (Hillock Morphology Index) number for 0.05 M and 0.1 M NaCl, 0.05 M and 0.1 M NaBr and 0.1 M $NaNO_3$ solutions with saturation index. All other solutions have HMI of 0.

Solution Name	***SI***	**HMI**	**Solution Name**	***SI***	**HMI**
Cl-1B	0.11	0.6	Br-2B	0.19	0.4
Cl-2B	0.2	0.8	Br-1A	0.09	0.8
Cl-3B	0.33	0.7	Br-2A	0.19	0.8
Cl-4B	0.4	0.6	Br-3A	0.29	0.8
Cl-5B	0.5	0.5	Br-4A	0.39	0.5
Cl-0A	0.05	1.4	Br-5A	0.49	0.6
Cl-2A	0.22	1.6	NO3-1A	0.11	0.6
Cl-3A	0.32	1.6	NO3-2A	0.21	0.4
Cl-4A	0.4	1.0	NO3-3A	0.33	0.6
Cl-5A	0.48	1.0	NO3-4A	0.41	0.4
Br-1B	0.1	0.2	NO3-5A	0.49	0.2

Statistical Analysis Results:

Table S2: Statistical comparison of the change in kinetic coefficient, $\Delta\beta$, and the 90% confidence interval bands. The interactions that are statistically significant are in bold.

Comparison of β: Ionic Strengths of Salts	**NaCl,** $\Delta\beta$, (90%CI)	**NaBr** $\Delta\beta$, (90%CI)	**$NaNO_3$** $\Delta\beta$, (90%CI)
0.01 M vs 0.05 M	3.5 (-3.9, 11) x 10^{-2}	**1.0 (0.21, 1.8) x 10^{-1}**	**7.1 (2.1, 12) x 10^{-2}**
0.01 M vs 0.1 M	**1.4 (0.8, 2.7) x 10^{-1}**	**9.5 (2.1, 17) x 10^{-2}**	**2.2 (0.21, 4.2) x 10^{-1}**
0.05 M vs 0.1 M	-1.0 (-2.3, 0.21) x 10^{-1}	6.7 (-69, 82) x 10^{-3}	-1.5 (-3.5,0.51) x 10^{-1}
Comparisons of β: Salts at Ionic strengths	**0.01 M** $\Delta\beta$, (90%CI)	**0.05 M** $\Delta\beta$, (90%CI)	**0.1M** $\Delta\beta$, (90%CI)
NaCl vs NaBr	**- 1.1 (-1.7, 0.42) x 10^{-1}**	- 4.0 (-19,11) x 10^{-2}	**- 1.5 (-2.3, -0.75) x 10^{-2}**
NaCl vs $NaNO_3$	**- 5.5 (-10, -1.1) x 10^{-2}**	- 2.0 (-11, 7.3) x 10^{-2}	2.7 (-12, 18) x 10^{-2}
NaBr vs $NaNO_3$	5.1 (-0.068, 10) x 10^{-2}	2.1 (-11, 15) x 10^{-2}	1.8 (0.11, 3.5) x 10^{-2}

The Intercept variable is the velocity-intercept (i.e., at zero barium activity) of the reference level (in this case NaCl) and the Activity is the slope (i.e., product of kinetic coefficient and molar volume) of the reference level (Table S2). The reference level is the variable that is included in the model while the categorical variable is held out of the model. Under TypeSalt or in this case Type NaBr, the parameter estimate is the difference between the reference level and categorical level intercepts. The interaction term (Int) is the difference in slopes between the reference level and categorical level.

Table S3: Weighted Least Squares Regression results for comparison of 0.01 M NaCl versus 0.01 M NaBr.

Parameter Estimates								
Variable	**Label**	**DF**	**Parameter Estimate**	**Standard Error**	**t Value**	**Pr > |t|**	**90% Confidence Limits**	
Intercept	Intercept	1	-2.01455	0.19280	-10.45	<.0001	-2.38919	-1.63991
Activity	Activity	1	116821	8661.94737	13.49	<.0001	99989	133653
TypeNaBr		1	1.26304	0.41753	3.02	0.0232	0.45169	2.07438
Int		1	-55348	17713	-3.12	0.0205	-89767	-20930

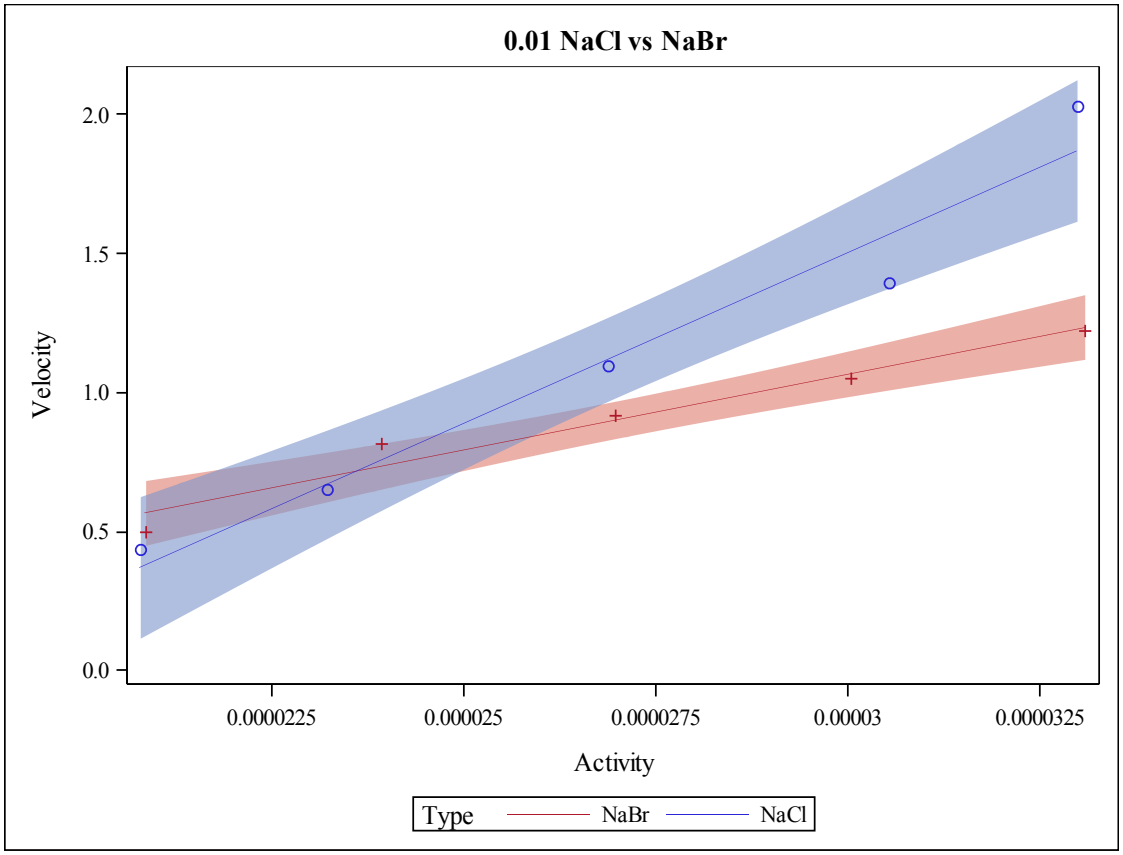

Figure S1: Velocity (nm/s) versus Barium Activity (M) for comparison of 0.01 M NaCl (circle) and 0.01 M NaBr (plus sign) with errors shaded.

Table S4: Weighted Least Squares Regression results for comparison of 0.01 M NaCl versus 0.01 M $NaNO_3$.

Parameter Estimates								
Variable	**Label**	**DF**	**Parameter Estimate**	**Standard Error**	**t Value**	**Pr > |t|**	**90% Confidence Limits**	
Intercept	Intercept	1	-2.01455	0.22844	-8.82	0.0001	-2.45846	-1.57064
Activity	Activity	1	116821	10264	11.38	<.0001	96877	136765
TypeNaNO3		1	0.45934	0.26877	1.71	0.1383	-0.06293	0.98161
Int		1	-28863	11929	-2.42	0.0519	-52044	-5681.80155

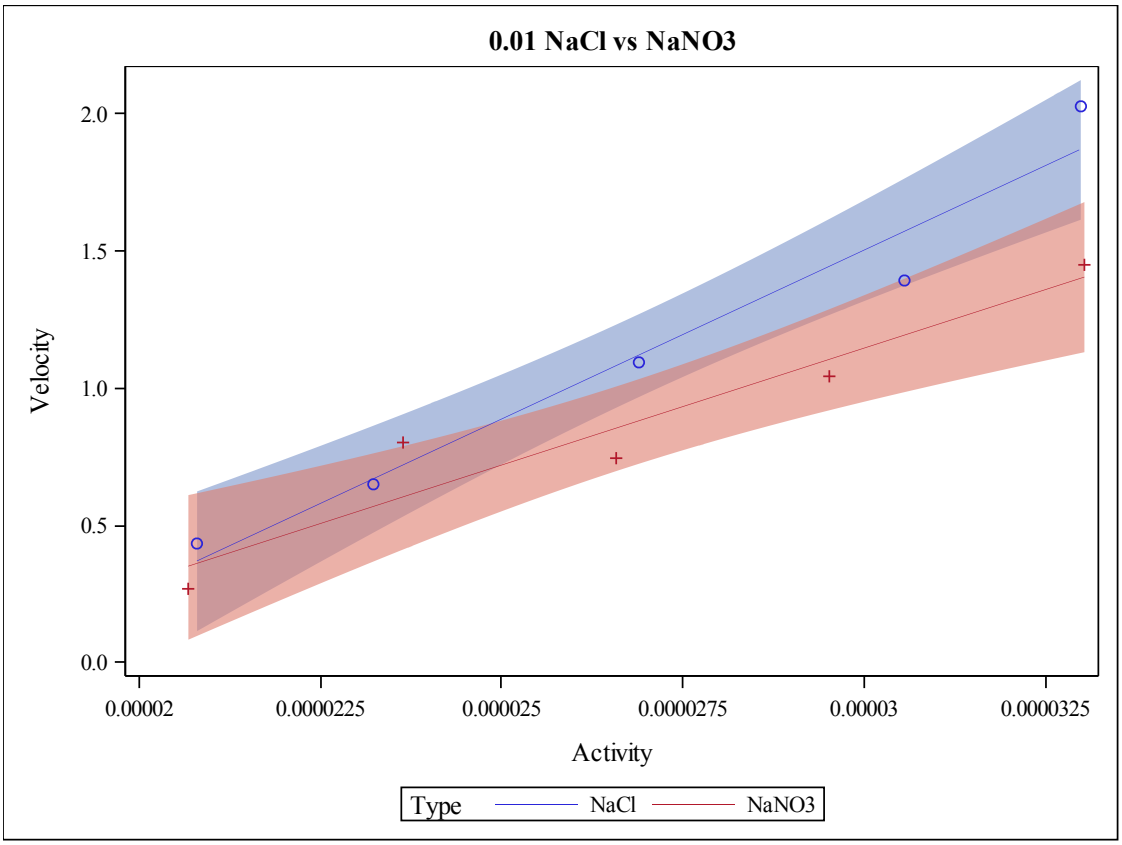

Figure S2: Velocity (nm/s) versus barium activity (M) for comparison of 0.01 M NaCl (circle) and 0.01 M $NaNO_3$ (plus sign) with errors shaded.

Table S5:Weighted Least Squares Regression results for comparison of 0.01 M $NaNO_3$ versus 0.01 M NaBr.

Parameter Estimates								
Variable	**Label**	**DF**	**Parameter Estimate**	**Standard Error**	**t Value**	**Pr > |t|**	**90% Confidence Limits**	
Intercept	Intercept	1	-0.75152	0.31422	-2.39	0.0539	-1.36210	-0.14093
Activity	Activity	1	61472	13108	4.69	0.0034	36000	86944
TypeNaNO3		1	-0.80370	0.33017	-2.43	0.0509	-1.44528	-0.16211
Int		1	26486	13813	1.92	0.1036	-354.66117	53326

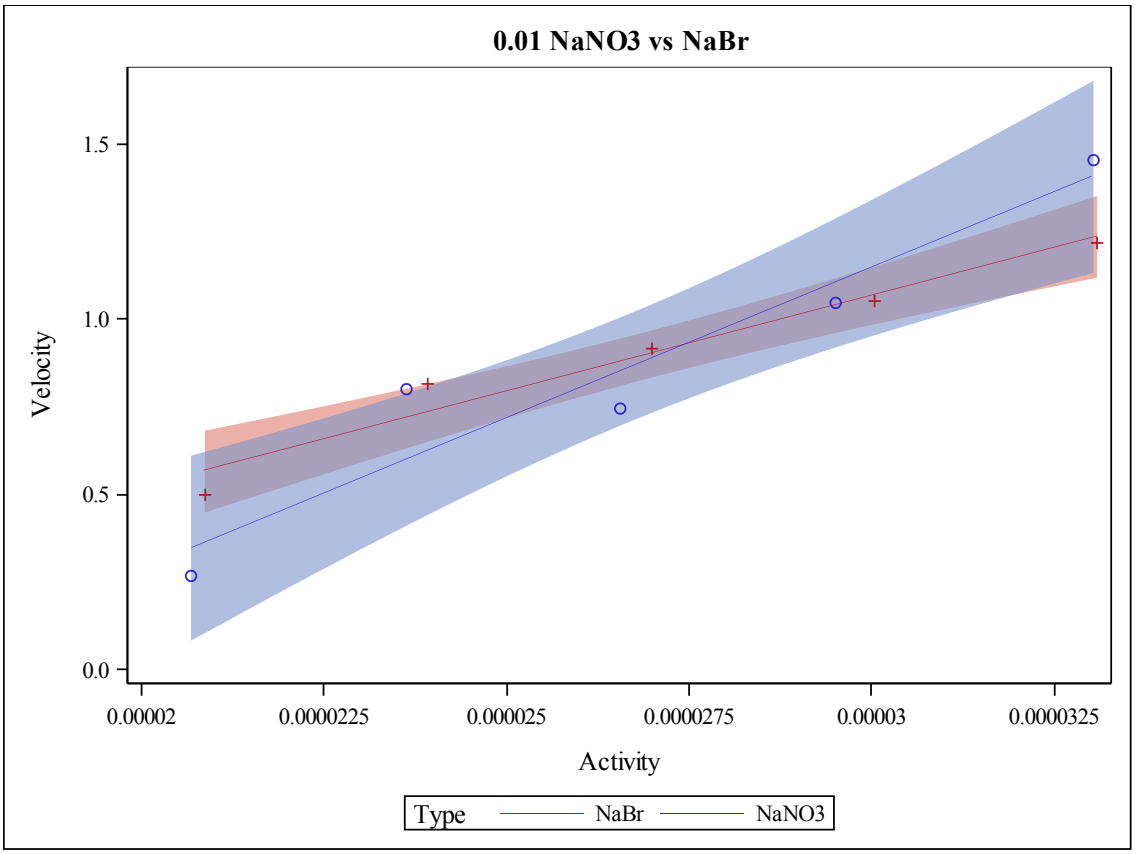

Figure S3: Velocity (nm/s) versus barium activity (M) for comparison of 0.01 M $NaNO_3$ (circle) and 0.01 M NaBr (plus sign) with errors shaded.

Table S6: Weighted Least Squares Regression results for comparison of 0.05 M NaCl versus 0.05 M NaBr.

Parameter Estimates								
Variable	**Label**	**DF**	**Parameter Estimate**	**Standard Error**	**t Value**	**Pr > |t|**	**90% Confidence Limits**	
Intercept	Intercept	1	-2.56771	0.34747	-7.39	0.0003	-3.24291	-1.89251
Activity	Activity	1	135274	15245	8.87	0.0001	105649	164899
TypeNaBr		1	0.78023	0.98591	0.79	0.4589	-1.13556	2.69603
Int		1	-21035	40470	-0.52	0.6218	-99676	57606

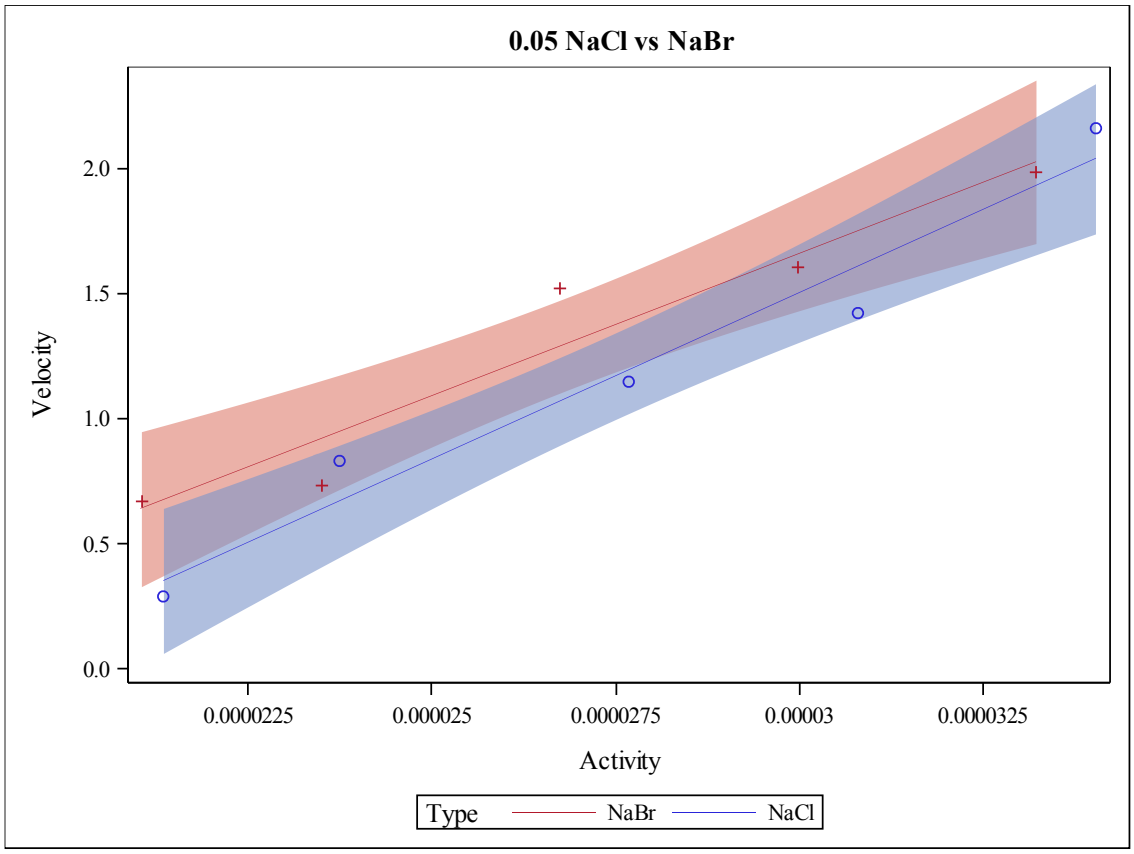

Figure S4: Velocity (nm/s) versus barium activity (M) for comparison of 0.05 M NaCl (circle) and 0.05 M NaBr (plus sign) with errors shaded.

Table S7: Weighted Least Squares Regression results for comparison of 0.05 M NaCl versus 0.05 M $NaNO_3$.

Parameter Estimates								
Variable	**Label**	**DF**	**Parameter Estimate**	**Standard Error**	**t Value**	**Pr > |t|**	**90% Confidence Limits**	
Intercept	Intercept	1	-2.56771	0.43027	-5.97	0.0010	-3.40381	-1.73161
Activity	Activity	1	135274	18878	7.17	0.0004	98590	171958
TypeNaNO3		1	0.38588	0.53878	0.72	0.5008	-0.66107	1.43284
Int		1	-10232	24905	-0.41	0.6955	-58627	38163

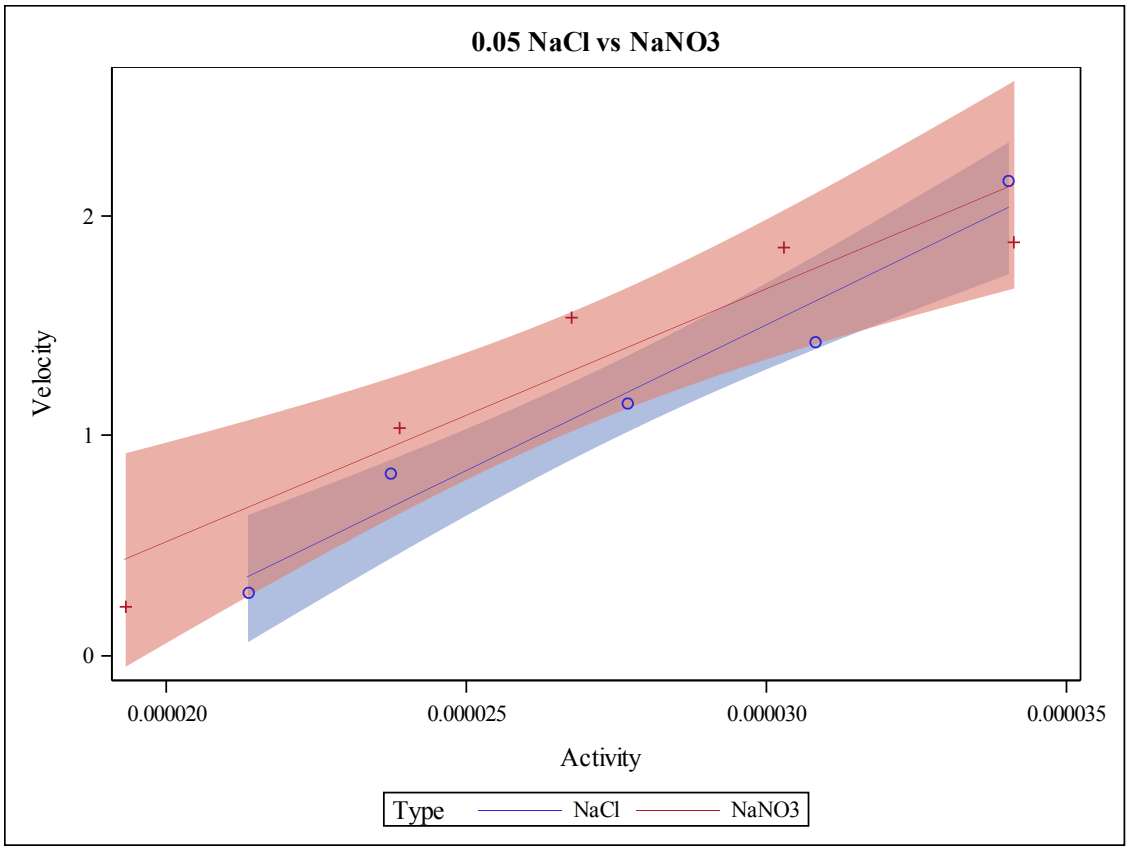

Figure S5: Velocity (nm/s) versus barium activity (M) for comparison of 0.05 M NaCl (circle) and 0.05 M $NaNO_3$ (plus sign) with errors shaded.

Table S8: Weighted Least Squares Regression results for comparison of 0.05 M NaBr versus 0.05 M $NaNO_3$.

Parameter Estimates								
Variable	**Label**	**DF**	**Parameter Estimate**	**Standard Error**	**t Value**	**Pr > |t|**	**90% Confidence Limits**	
Intercept	Intercept	1	-1.78747	0.82331	-2.17	0.0730	-3.38732	-0.18763
Activity	Activity	1	114239	33453	3.41	0.0142	49234	179244
TypeNaNO3		1	-0.39435	0.85583	-0.46	0.6612	-2.05739	1.26869
Int		1	10803	35442	0.30	0.7708	-58067	79673

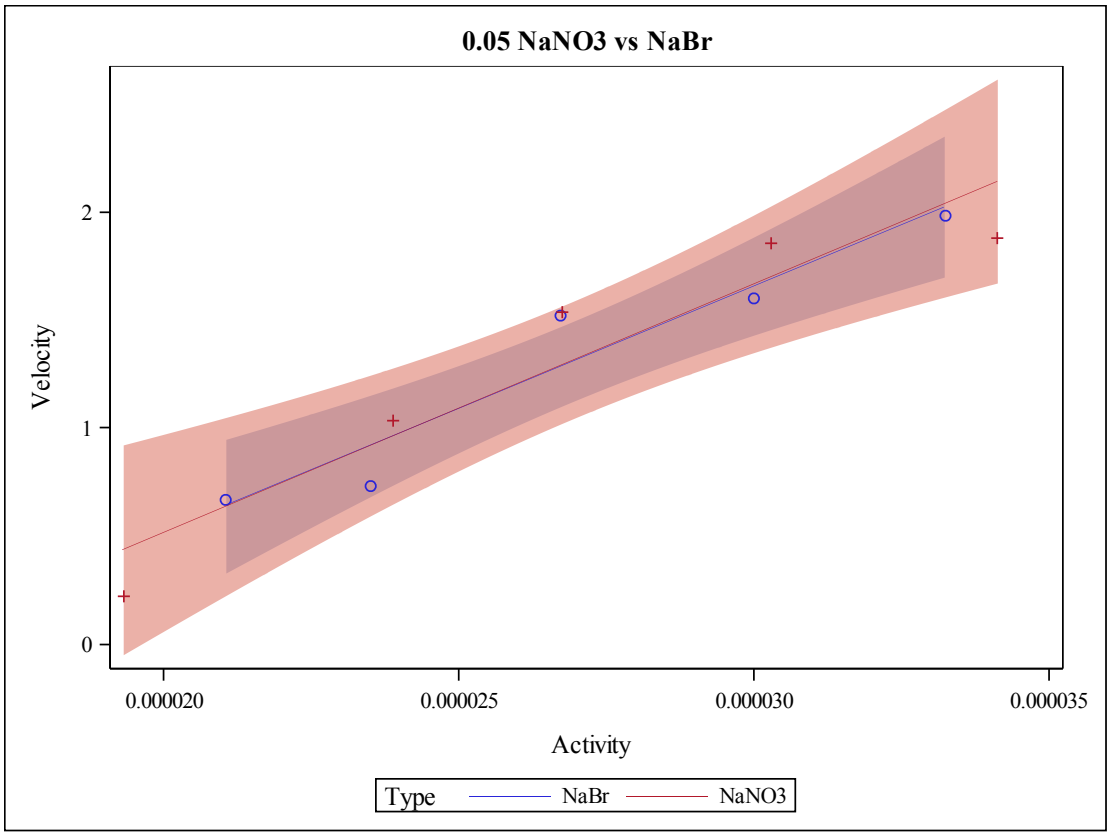

Figure S6: Velocity (nm/s) versus barium activity (M) for comparison of 0.05 M NaBr (circle) and 0.05 M $NaNO_3$ (plus sign) with errors shaded.

Table S9: Weighted Least Squares Regression results for comparison of 0.1 M NaCl versus 0.1 M NaBr.

Parameter Estimates								
Variable	**Label**	**DF**	**Parameter Estimate**	**Standard Error**	**t Value**	**Pr > |t|**	**90% Confidence Limits**	
Intercept	Intercept	1	-3.53193	0.34423	-10.26	<.0001	-4.20083	-2.86303
Activity	Activity	1	189599	16168	11.73	<.0001	158182	221017
TypeNaBr		1	2.09452	0.46336	4.52	0.0040	1.19413	2.99490
Int		1	-78826	20518	-3.84	0.0085	-118697	-38955

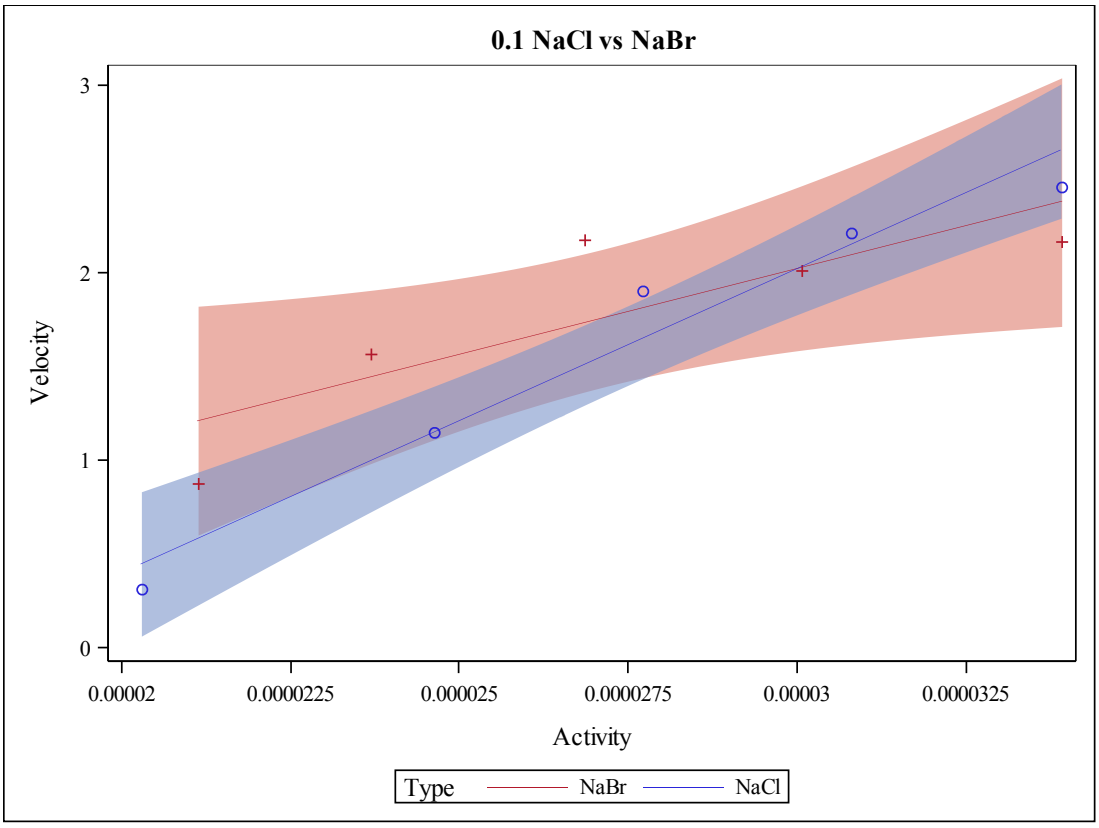

Figure S7: Velocity (nm/s) versus barium activity (M) for comparison of 0.1 M NaCl (circle) and 0.1 M NaBr (plus sign) with errors shaded.

Table S10: Weighted Least Squares Regression results for comparison of 0.1 M NaCl versus 0.1 M $NaNO_3$.

Parameter Estimates								
Variable	**Label**	**DF**	**Parameter Estimate**	**Standard Error**	**t Value**	**Pr > |t|**	**90% Confidence Limits**	
Intercept	Intercept	1	-3.53193	0.42048	-8.40	0.0002	-4.34899	-2.71487
Activity	Activity	1	189599	19749	9.60	<.0001	151223	227976
TypeNaNO3		1	-0.02015	0.94608	-0.02	0.9837	-1.85854	1.81825
Int		1	14252	40088	0.36	0.7344	-63647	92151

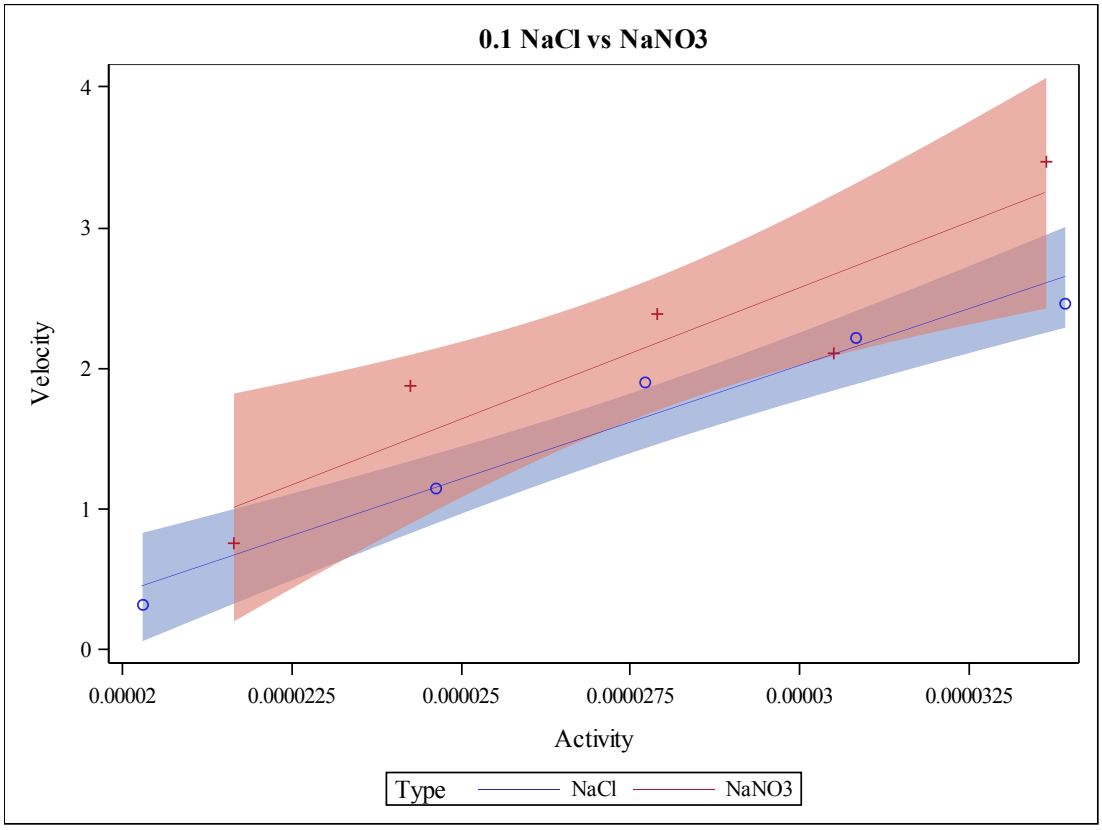

Figure S8: Velocity (nm/s) versus barium activity (M) for comparison of 0.1 M NaCl (circle) and 0.1 M $NaNO_3$ (plus sign) with errors shaded.

Table S11: Weighted Least Squares Regression results for comparison of 0.1 M NaBr versus 0.1 M $NaNO_3$.

Parameter Estimates								
Variable	**Label**	**DF**	**Parameter Estimate**	**Standard Error**	**t Value**	**Pr > |t|**	**90% Confidence Limits**	
Intercept	Intercept	1	-1.43742	0.44608	-3.22	0.0181	-2.30423	-0.57060
Activity	Activity	1	110773	18169	6.10	0.0009	75467	146079
TypeNaNO3		1	-2.11466	1.09301	-1.93	0.1012	-4.23859	0.00926
Int		1	93079	44914	2.07	0.0836	5802.53964	180355

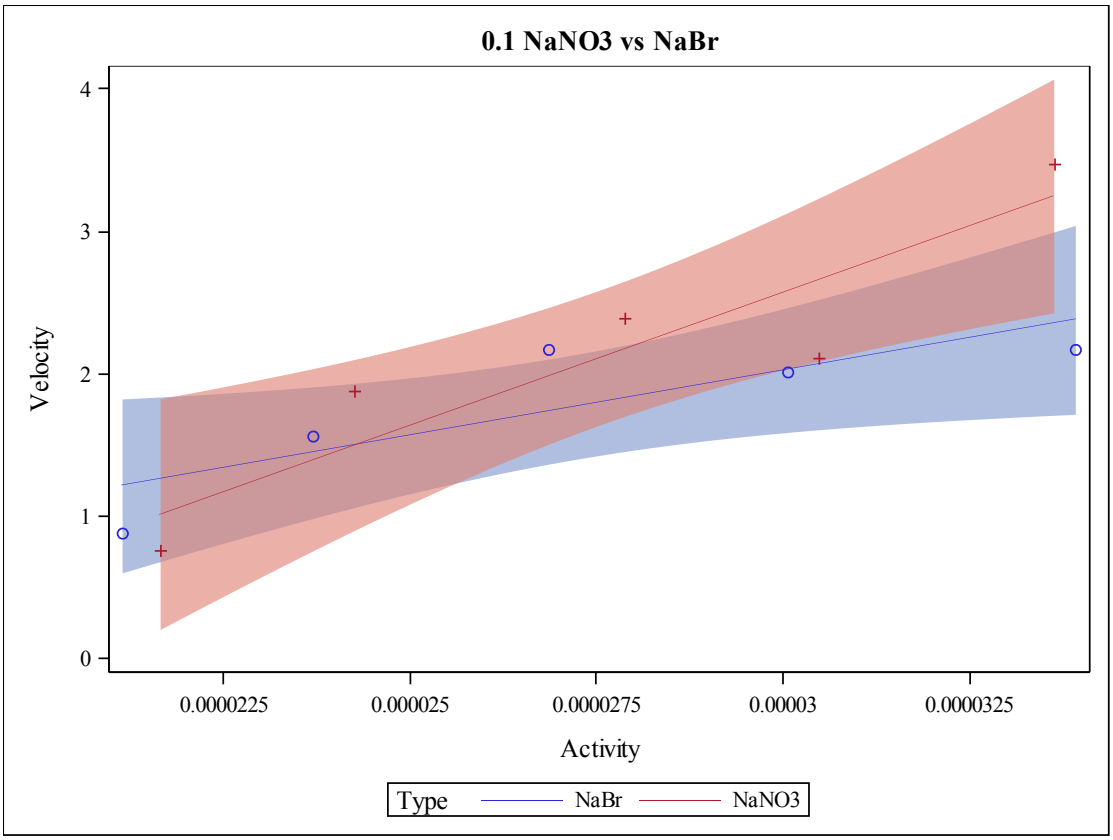

Figure S9: Velocity (nm/s) versus barium activity (M) for comparison of 0.1 M NaBr (circle) and 0.1 M $NaNO_3$ (plus sign) with errors shaded.

Table S12: Weighted Least Squares Regression for NaCl Comparison with 0.01 M NaCl as the reference point.

Parameter Estimates								
Variable	**Label**	**DF**	**Parameter Estimate**	**Standard Error**	**t Value**	**Pr > |t|**	**90% Confidence Limits**	
Intercept	Intercept	1	-2.01455	0.37560	-5.36	0.0005	-2.70306	-1.32604
Activity	Activity	1	116821	16875	6.92	<.0001	85888	147754
M05		1	-0.55316	0.47587	-1.16	0.2750	-1.42548	0.31917
M1		1	-1.51738	0.80255	-1.89	0.0912	-2.98854	-0.04622
Int05		1	18453	21192	0.87	0.4065	-20395	57301
Int1		1	72779	37342	1.95	0.0831	4326.59891	141230

Table S13: Weighted Least Squares Regression for NaCl Comparison with 0.1 M NaCl as the reference point.

Parameter Estimates								
Variable	**Label**	**DF**	**Parameter Estimate**	**Standard Error**	**t Value**	**Pr > |t|**	**90% Confidence Limits**	
Intercept	Intercept	1	-3.53193	0.70923	-4.98	0.0008	-4.83203	-2.23183
Activity	Activity	1	189599	33312	5.69	0.0003	128535	250663
M01		1	1.51738	0.80255	1.89	0.0912	0.04622	2.98854
M05		1	0.96422	0.76706	1.26	0.2404	-0.44189	2.37034
Int01		1	-72779	37342	-1.95	0.0831	-141230	-4326.59891
Int05		1	-54325	35693	-1.52	0.1623	-119755	11105

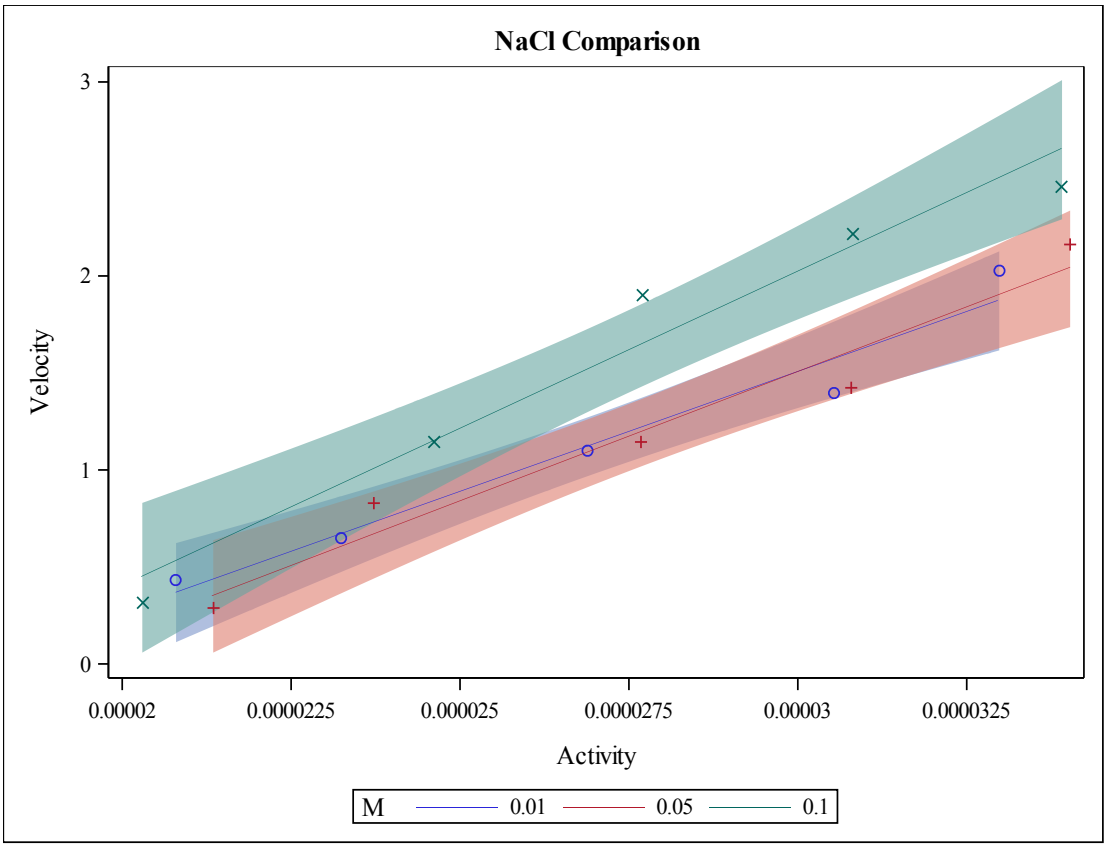

Figure S10: Velocity (nm/s) versus barium activity (M) for 0.01 M (circle), 0.05 M (plus) and 0.1 M (x) NaCl solutions.

Table S14: Weighted Least Squares Regression for NaBr Comparison with 0.01 M NaBr as the reference point.

Parameter Estimates								
Variable	**Label**	**DF**	**Parameter Estimate**	**Standard Error**	**t Value**	**Pr > |t|**	**90% Confidence Limits**	
Intercept	Intercept	1	-0.75152	0.37866	-1.98	0.0785	-1.44564	-0.05739
Activity	Activity	1	61472	15797	3.89	0.0037	32515	90429
M05		1	-1.03596	0.55605	-1.86	0.0953	-2.05527	-0.01665
M1		1	-0.68590	0.50584	-1.36	0.2081	-1.61316	0.24136
Int05		1	52767	22875	2.31	0.0465	10834	94700
Int1		1	49301	20884	2.36	0.0426	11018	87584

Table S15: Weighted Least Squares Regression for NaBr Comparison with 0.1 M NaBr as the reference point.

Parameter Estimates								
Variable	**Label**	**DF**	**Parameter Estimate**	**Standard Error**	**t Value**	**Pr > |t|**	**90% Confidence Limits**	
Intercept	Intercept	1	-1.43742	0.33539	-4.29	0.0020	-2.05222	-0.82261
Activity	Activity	1	110773	13661	8.11	<.0001	85732	135814
M05		1	-0.35006	0.52754	-0.66	0.5236	-1.31710	0.61698
M01		1	0.68590	0.50584	1.36	0.2081	-0.24136	1.61316
Int05		1	3466.26073	21456	0.16	0.8752	-35865	42798
Int01		1	-49301	20884	-2.36	0.0426	-87584	-11018

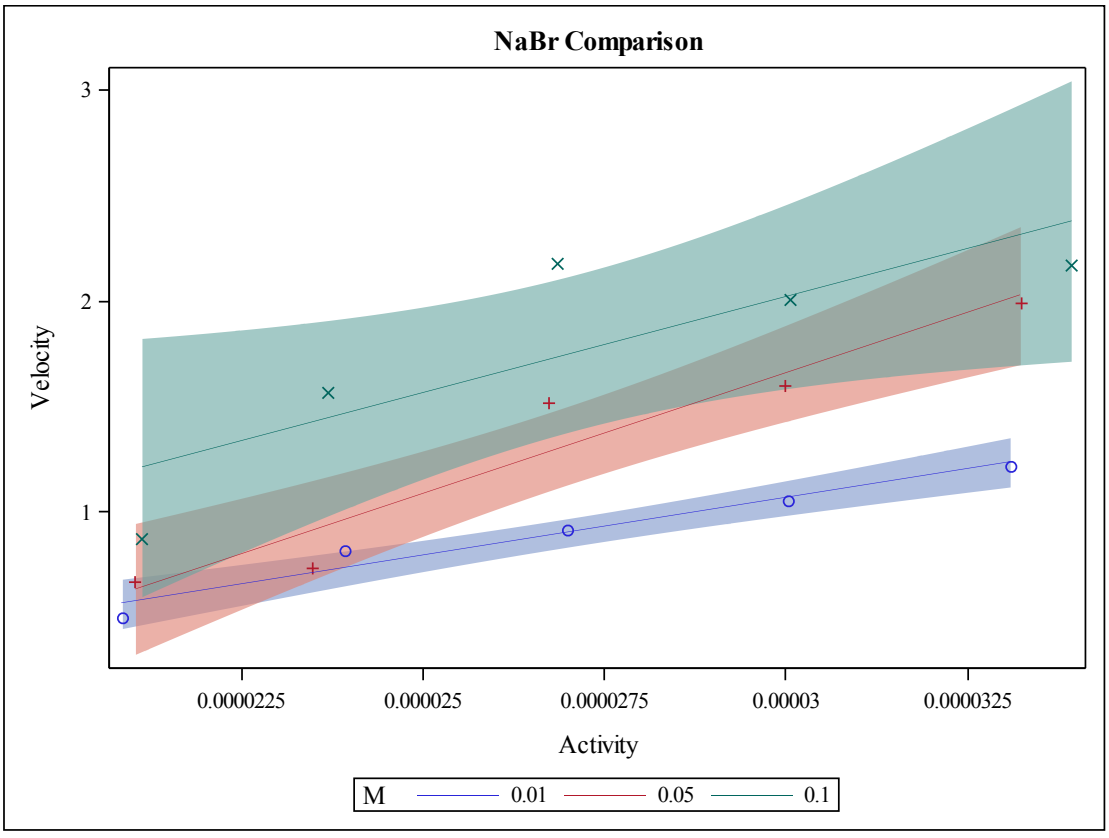

Figure S11: Velocity (nm/s) versus barium activity (M) for 0.01 M (circle), 0.05 M (plus) and 0.1 M (x) NaBr solutions.

Table S16: Weighted Least Squares Regression for $NaNO_3$ Comparison with 0.01 M $NaNO_3$ as the reference point.

Parameter Estimates								
Variable	**Label**	**DF**	**Parameter Estimate**	**Standard Error**	**t Value**	**Pr > |t|**	**90% Confidence Limits**	
Intercept	Intercept	1	-1.55521	0.22409	-6.94	<.0001	-1.96600	-1.14443
Activity	Activity	1	87958	9622.91581	9.14	<.0001	70318	105598
M05		1	-0.62661	0.30846	-2.03	0.0728	-1.19205	-0.06117
M1		1	-1.99687	1.39410	-1.43	0.1858	-4.55241	0.55868
Int05		1	37084	14330	2.59	0.0293	10816	63353
Int1		1	115894	57452	2.02	0.0745	10578	221209

Table S17: Weighted Least Squares Regression for $NaNO_3$ Comparison with 0.1 M $NaNO_3$ as the reference point.

Parameter Estimates								
Variable	**Label**	**DF**	**Parameter Estimate**	**Standard Error**	**t Value**	**Pr > |t|**	**90% Confidence Limits**	
Intercept	Intercept	1	-3.55208	1.37597	-2.58	0.0296	-6.07440	-1.02976
Activity	Activity	1	203851	56640	3.60	0.0058	100023	307679
M01		1	1.99687	1.39410	1.43	0.1858	-0.55868	4.55241
M05		1	1.37025	1.39221	0.98	0.3507	-1.18182	3.92233
Int01		1	-115894	57452	-2.02	0.0745	-221209	-10578
Int05		1	-78809	57627	-1.37	0.2046	-184446	26827

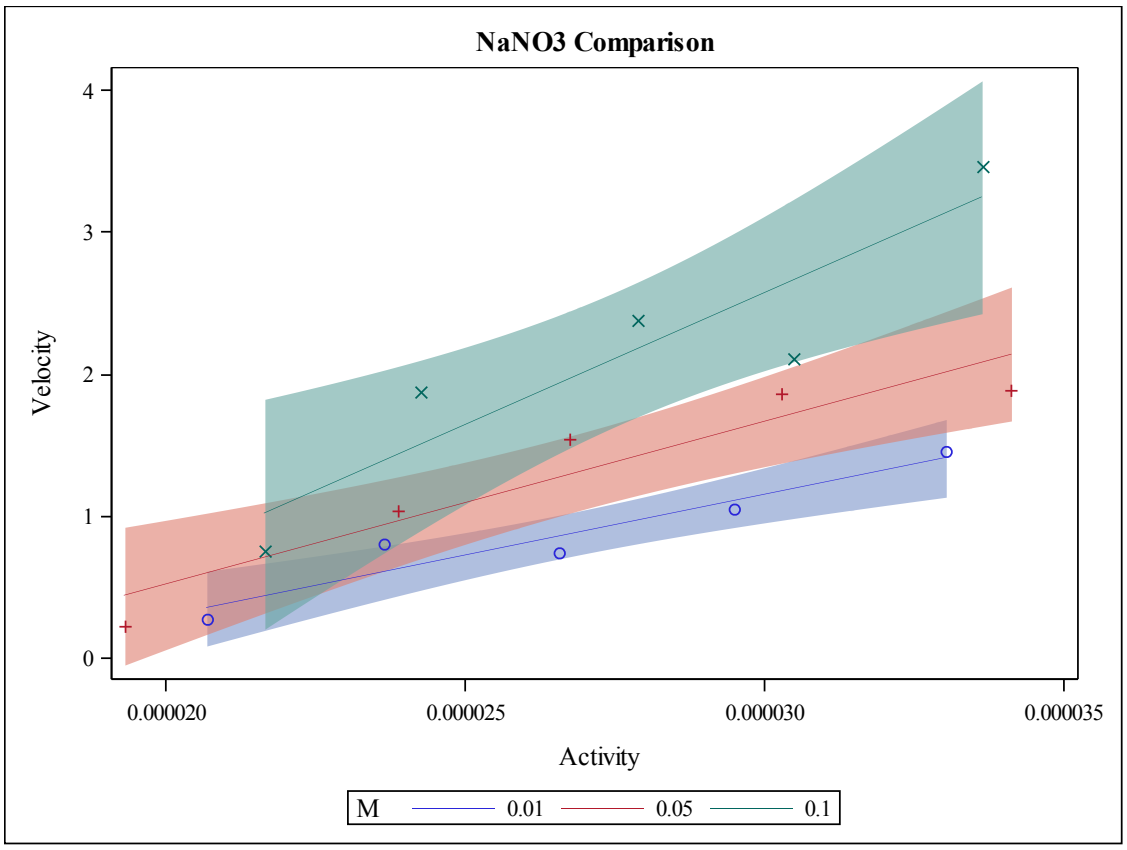

Figure S12: Velocity (nm/s) versus barium activity (M) for 0.01 M (◦), 0.05 M (plus sign) and 0.1 M (x) $NaNO_3$ solutions.

Solution Stability: HAFM Background Electrolyte with r > 1.

Table S18: Solution composition for HAFM experiments of barite growth with r >1.

Runs	mL Na_2SO_4 Added°	mL $BaCl_2$ Added•	mL NaCl Added*	$[Ba^{2+}]$ (x 10^{-4})	$[SO_4^{2-}]$ (x 10^{-5})	$\{Ba^{2+}\}$ (x 10^{-5}) (M)	*SI*	r ($[Ba^{2+}]/[SO_4^{2-}]$)	*I* (x 10^{-2}) (M)	Average ⟨120⟩ Step Velocity (nm/s)	Standard Deviation of Step Velocity
Cl-1A	0.240	0.590	49.170	1.13	4.05	3.62	0.11	2.79	9.78	0.50	0.2
Cl-2A	0.250	0.610	49.140	1.17	4.21	3.74	0.15	2.77	9.77	1.61	0.59
Cl-3A	0.275	0.675	49.050	1.29	4.64	4.14	0.23	2.78	9.76	0.97	0.13
Cl-5A	0.310	0.750	48.940	1.44	5.23	4.60	0.33	2.75	9.75	2.06	0.21
Cl-5A	0.310	0.750	48.940	1.44	5.23	4.60	0.33	2.75	9.75	1.62	0.25
Cl-6A	0.340	0.825	48.835	1.58	5.73	5.07	0.41	2.75	9.73	1.81	0.22
Cl-7A	0.360	0.875	48.765	1.67	6.07	5.38	0.46	2.76	9.72	2.59	0.35
Cl-8A	0.380	0.925	48.695	1.77	6.41	5.68	0.51	2.76	9.71	2.66	0.65
Cl-9A	0.410	1.000	48.590	1.91	6.75	6.15	0.57	2.84	9.70	3.89	0.61
Cl-10A	0.450	1.100	48.450	2.11	7.60	6.77	0.66	2.77	9.68	3.56	0.25
Cl-11A	0.470	1.150	48.380	2.20	7.94	7.08	0.7	2.77	9.67	3.10	0.61
Cl-12A	0.480	1.180	48.340	2.26	8.10	7.27	0.72	2.79	9.66	4.07	0.67

Footnote: The concentration (M) of the stock solutions for Cl-A experiments are (°) 0.0100 M, (•) 0.00999 M and (*) 0.100 M.

Runs	mL Na_2SO_4 Added°	mL $BaCl_2$ Added•	mL NaCl Added*	$[Ba^{2+}]$ (x 10^{-4})	$[SO_4^{2-}]$ (x 10^{-5})	$\{Ba^{2+}\}$ (x 10^{-5}) (M)	*SI*	r ($[Ba^{2+}]/[SO_4^{2-}]$)	*I* (x 10^{-2}) (M)	Average ⟨120⟩ Step Velocity (nm/s)	Standard Deviation of Step Velocity
Cl-2B	0.190	0.485	49.325	0.94	3.39	3.82	0.18	2.78	4.94	1.13	0.40
Cl-3B	0.205	0.525	49.270	1.02	3.65	4.14	0.24	2.79	4.94	1.70	0.18
Cl-4B	0.215	0.550	49.235	1.07	3.83	4.33	0.28	2.79	4.93	2.65	0.53
Cl-5B	0.235	0.600	49.165	1.17	4.19	4.73	0.36	2.78	4.93	3.07	0.35
Cl-6B	0.255	0.650	49.095	1.26	4.55	5.12	0.43	2.78	4.93	3.46	0.51
Cl-7B	0.275	0.700	49.025	1.36	4.90	5.52	0.5	2.78	4.93	5.73	1.58
Cl-8B	0.295	0.750	48.955	1.46	5.26	5.92	0.56	2.77	4.92	3.88	0.47
Cl-9B	0.310	0.800	48.890	1.56	5.53	6.31	0.61	2.81	4.92	4.30	0.44
Cl-10B	0.330	0.850	48.820	1.65	5.89	6.71	0.66	2.81	4.92	5.39	0.57
Cl-11B	0.340	0.875	48.785	1.70	6.06	6.91	0.69	2.81	4.92	4.48	0.42

Footnote: The concentration (M) of the stock solutions for Cl-B experiments are (°) 0.0100 M, (•) 0.00999 M and (*) 0.0501 M.

Runs	**mL Na_2SO_4 Added°**	**mL $BaCl_2$ Added•**	**mL NaCl Added***	**[Ba^{2+}] (x 10^{-5})**	**[SO_4^{2-}] (x 10^{-5})**	**{Ba^{2+}} (x 10^{-5}) (M)**	***SI***	**r ([Ba^{2+}]/ [SO_4^{2-}])**	***I*** **(x 10^{-2}) (M)**	**Average ⟨120⟩ Step Velocity (nm/s)**	**Standard Deviation of Step Velocity**
Cl-3C	0.120	0.340	49.540	6.74	2.31	4.15	0.24	2.92	1.03	0.59	0.04
Cl-5C	0.140	0.395	49.465	7.83	2.70	4.81	0.38	2.90	1.03	1.09	0.08
Cl-6C	0.150	0.420	49.430	8.33	2.89	5.12	0.43	2.88	1.03	1.61	0.22
Cl-8C	0.170	0.475	49.355	9.42	3.28	5.78	0.54	2.88	1.03	1.70	0.11
Cl-9C	0.180	0.500	49.320	9.91	3.47	6.09	0.59	2.86	1.03	2.40	0.24
Cl-10C	0.200	0.550	49.250	10.9	3.85	6.69	0.67	2.83	1.04	2.41	0.12
Cl-12C	0.215	0.600	49.185	11.9	4.14	7.30	0.74	2.87	1.04	2.82	0.21

Footnote: The concentration (M) of the stock solutions for Cl-C experiments are (°) 0.0100 M, (•) 0.0100 M and (*) 0.0102 M.

Runs	mL Na_2SO_4 Added°	mL $BaCl_2$ Added•	mL NaBr Added*	$[Ba^{2+}]$ (x 10^{-4})	$[SO_4^{2-}]$ (x 10^{-5})	$\{Ba^{2+}\}$ (x 10^{-5}) (M)	*SI*	r ($[Ba^{2+}]/[SO_4^{2-}]$)	*I* (x 10^{-2}) (M)	Average ⟨120⟩ Step Velocity (nm/s)	Standard Deviation of Step Velocity
Br-1A	0.285	0.47	49.245	0.95	4.79	3.00	0.1	2.19	9.99	0.59	0.19
Br-3A	0.32	0.53	49.150	1.07	5.38	3.39	0.21	2.16	9.98	1.08	0.39
Br-5A	0.36	0.59	49.050	1.19	6.06	3.77	0.3	2.14	9.96	0.74	0.18
Br-7A	0.405	0.67	48.925	1.35	6.82	4.23	0.41	2.13	9.94	1.61	0.87
Br-10A	0.48	0.79	48.730	1.59	8.08	5.06	0.56	2.14	9.92	2.41	0.35

Footnote: The concentration (M) of the stock solutions for Br-A experiments are (°) 0.0100 M, (•) 0.0100 M and (*) 0.101 M.

Runs	mL Na_2SO_4 Added°	mL $BaCl_2$ Added•	mL NaBr Added*	$[Ba^{2+}]$ (x 10^{-5})	$[SO_4^{2-}]$ (x 10^{-5})	$\{Ba^{2+}\}$ (x 10^{-5}) (M)	*SI*	r($[Ba^{2+}]/[SO_4^{2-}]$)	*I* (x 10^{-2}) (M)	Average ⟨120⟩ Step Velocity (nm/s)	Standard Deviation of Step Velocity
Br-1B	0.22	0.38	49.400	7.64	3.91	3.08	0.14	2.06	5.03	0.73	0.06
Br-3B	0.24	0.42	49.340	8.44	4.27	3.40	0.22	2.09	5.03	0.91	0.05
Br-5B	0.27	0.47	49.260	9.45	4.81	3.81	0.32	2.08	5.03	1.17	0.08
Br-7B	0.3	0.53	49.170	10.7	5.34	4.30	0.42	2.11	5.02	1.31	0.09
Br-10B	0.36	0.63	49.010	12.7	6.41	5.11	0.58	2.08	5.01	1.90	0.20

Footnote: The concentration (M) of the stock solutions for Br-B experiments are (°) 0.0100 M, (•) 0.0100 M and (*) 0.0505 M.

Runs	mL Na_2SO_4 Added°	mL $BaCl_2$ Added•	mL NaBr Added*	$[Ba^{2+}]$ (x 10^{-5})	$[SO_4^{2-}]$ (x 10^{-5})	$\{Ba^{2+}\}$ (x 10^{-5}) (M)	*SI*	r($[Ba^{2+}]/[SO_4^{2-}]$)	*I* (x10^{-2}) (M)	Average ⟨120⟩ Step Velocity (nm/s)	Standard Deviation of Step Velocity
Br-1C	0.13	0.245	49.625	4.93	2.50	3.01	0.14	2.00	1.06	0.57	0.21
Br-3C	0.145	0.275	49.580	5.53	2.79	3.37	0.23	2.01	1.06	0.98	0.19
Br-5C	0.16	0.300	49.540	6.03	3.08	3.68	0.31	1.99	1.07	0.60	0.15
Br-7C	0.18	0.340	49.480	6.83	3.46	4.17	0.42	2.00	1.07	1.72	0.38
Br-10C	0.215	0.405	49.380	8.14	4.14	4.96	0.57	2.00	1.07	1.85	0.33

Footnote: The concentration (M) of the stock solutions for Br-C experiments are (°) 0.0100 M, (•) 0.0100 M and (*) 0.0105 M.

Runs	mL Na_2SO_4 Added°	mL $BaCl_2$ Added•	mL $NaNO_3$ Added*	$[Ba^{2+}]$ (x 10^{-5})	$[SO_4^{2-}]$ (x 10^{-5})	$\{Ba^{2+}\}$ (x 10^{-5}) (M)	*SI*	r($[Ba^{2+}]$/ $[SO_4^{2-}]$)	*I* (x 10^{-2}) (M)	Average ⟨120⟩ Step Velocity (nm/s)	Standard Deviation of Step Velocity
NO3-0A	0.270	0.475	49.255	7.67	4.54	2.44	-0.01	1.84	9.99	0.18	0.02
NO3-1A	0.285	0.500	49.215	8.08	4.80	2.57	0.03	1.84	9.98	0.46	0.08
NO3-2A	0.300	0.525	49.175	8.48	5.05	2.70	0.08	1.83	9.97	0.67	0.09
NO3-3A	0.320	0.565	49.115	9.13	5.39	2.90	0.14	1.85	9.97	0.96	0.12
NO3-4A	0.340	0.595	49.065	9.61	5.72	3.06	0.19	1.83	9.96	1.50	0.55
NO3-5A	0.360	0.630	49.010	10.2	6.06	3.24	0.24	1.83	9.95	1.47	0.16
NO3-6A	0.380	0.670	48.950	10.8	6.40	3.45	0.29	1.85	9.94	1.15	0.24
NO3-7A	0.400	0.705	48.895	11.4	6.73	3.63	0.33	1.85	9.93	2.07	0.19
NO3-8A	0.430	0.750	48.820	12.1	7.24	3.86	0.39	1.83	9.92	2.58	0.46
NO3-9A	0.450	0.790	48.760	12.8	7.58	4.07	0.43	1.84	9.91	2.30	1.14
NO3-10A	0.480	0.840	48.680	13.6	8.09	4.33	0.49	1.83	9.90	2.10	0.37

Footnote: The concentration (M) of the stock solutions for NO_3-A experiments are (°) 0.0100 M, (•) 0.0100 M and (*) 0.101 M.

Runs	mL Na_2SO_4 Added°	mL $BaCl_2$ Added•	mL $NaNO_3$ Added*	$[Ba^{2+}]$ (x 10^{-5})	$[SO_4^{2-}]$ (x 10^{-5})	$\{Ba^{2+}\}$ (x 10^{-5}) (M)	*SI*	r($[Ba^{2+}]$/ $[SO_4^{2-}]$)	*I* (x 10^{-2}) (M)	Average ⟨120⟩ Step Velocity (nm/s)	Standard Deviation of Step Velocity
NO3-0B	0.200	0.365	49.435	6.34	3.56	2.56	0.02	1.88	4.99	0.16	0.02
NO3-1B	0.215	0.390	49.395	6.78	3.83	2.74	0.08	1.87	4.98	0.48	0.05
NO3-2B	0.220	0.405	49.375	7.04	3.92	2.85	0.11	1.90	4.98	0.43	0.05
NO3-3B	0.240	0.435	49.325	7.56	4.28	3.06	0.18	1.87	4.98	0.56	0.09
NO3-4B	0.250	0.460	49.290	8.00	4.45	3.23	0.22	1.89	4.98	0.66	0.03
NO3-5B	0.270	0.490	49.240	8.52	4.81	3.45	0.28	1.87	4.98	0.85	0.08
NO3-6B	0.285	0.515	49.200	8.96	5.08	3.62	0.33	1.86	4.98	1.07	0.13
NO3-7B	0.300	0.545	49.155	9.48	5.35	3.83	0.37	1.87	4.97	1.39	0.20
NO3-8B	0.315	0.575	49.110	10.0	5.61	4.05	0.42	1.88	4.97	1.33	0.10
NO3-9B	0.335	0.610	49.055	10.6	5.97	4.29	0.47	1.88	4.97	1.54	0.15

Footnote: The concentration (M) of the stock solutions for NO_3-B experiments are (°) 0.0100 M, (•) 0.0100 M and (*) 0.0500 M.

Runs	mL Na_2SO_4 Added°	mL $BaCl_2$ Added•	mL $NaNO_3$ Added*	$[Ba^{2+}]$ (x 10^{-5})	$[SO_4^{2-}]$ (x 10^{-5})	$\{Ba^{2+}\}$ (x 10^{-5}) (M)	*SI*	r($[Ba^{2+}]$/ $[SO_4^{2-}]$)	*I* (x 10^{-2}) (M)	Average ⟨120⟩ Step Velocity (nm/s)	Standard Deviation of Step Velocity
NO3-2C	0.135	0.255	49.610	4.89	2.60	3.01	0.16	1.91	1.02	0.35	0.02
NO3-3C	0.140	0.270	49.590	5.18	2.70	3.19	0.2	1.95	1.02	0.63	0.03
NO3-5C	0.160	0.305	49.535	5.85	3.08	3.60	0.31	1.92	1.02	0.47	0.02
NO3-6C	0.170	0.320	49.510	6.14	3.28	3.78	0.36	1.90	1.02	1.13	0.07
NO3-7C	0.180	0.340	49.480	6.52	3.47	4.01	0.41	1.91	1.02	1.08	0.30
NO3-9 C	0.200	0.385	49.415	7.38	3.85	4.54	0.51	1.94	1.02	0.82	0.04
NO3-10C	0.215	0.405	49.380	7.77	4.14	4.78	0.56	1.90	1.03	1.75	0.08

Footnote: The concentration (M) of the stock solutions for NO_3-C experiments are (°) 0.0100 M, (•) 0.0100 M and (*) 0.0100 M.

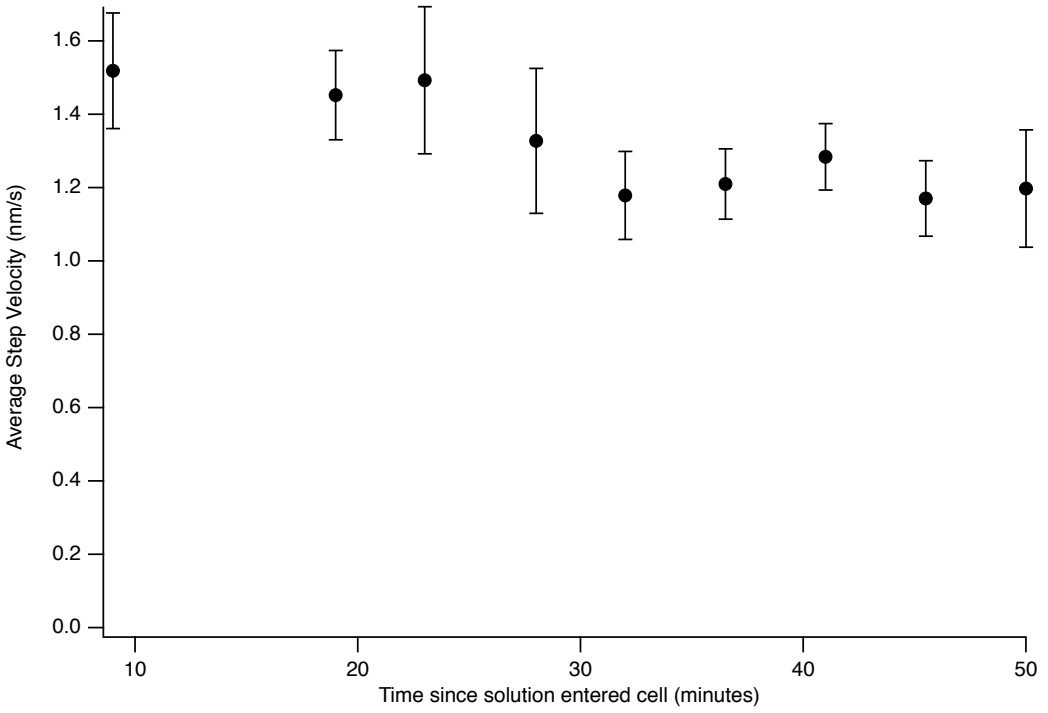

Figure S13: Average step velocity (nm/s) versus minutes since injection of the Br-3B solution. In around 50 minutes of the solution entering the cell, the step velocity decreased by ~0.3 nm/s. This is a solution that is in the middle in terms of *SI* and *I*. More investigation into timing of data is needed.

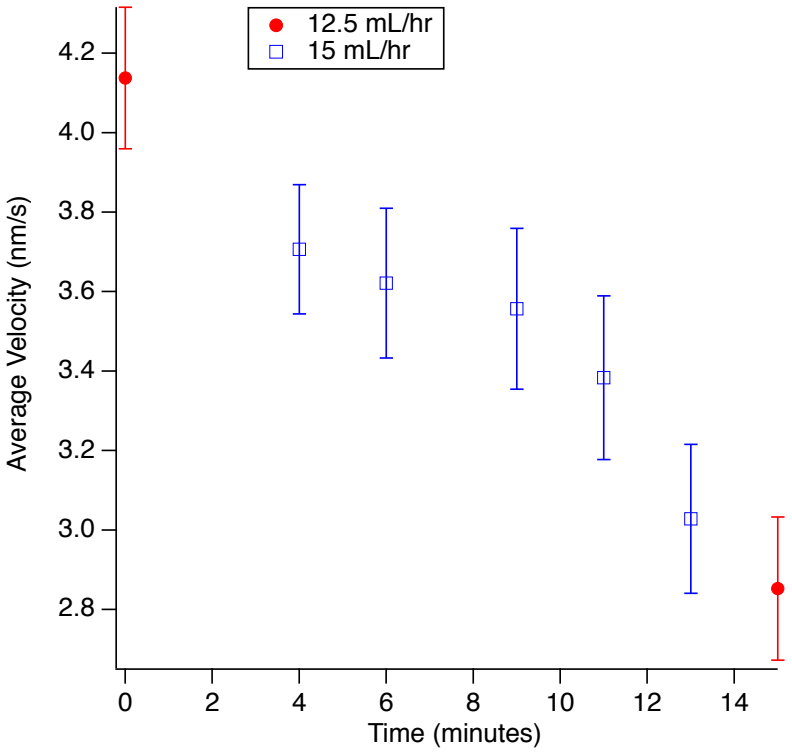

Figure S14: Average velocity (nm/s) versus Time (minute) since Data Collection for 10-ClA solution (r >1) showing velocities over a flow rate change (12.5 mL/hr to 15 mL/hr). A flow rate of 12.5 mL/hr does not limit the rate of crystal growth. There is an apparent decrease in step velocities over the first 15 minutes the solution is introduced into the fluid cell. The change in velocity over a 15 minute time period is 1.28 nm/s.

Timing of Data: Sodium Chloride

Experiments have shown that over a time span of tens of minutes, the step velocities for some solutions, particularly ones with higher saturation indices, decrease over this time period. Step velocities at two different times were analyzed to determine if the step velocities had statistically decreased in a 20-30 minute time span. Step velocities between 6-10 minutes after the solution had been switched in and at least 10 to 20 minutes later were compared. This could be due to higher barium activity and higher ratio of barium to sulfate for sodium chloride solutions. Each ionic strength was examined and solutions were omitted from the overall data set due to solution stability issues. For the sodium chloride

data, solutions 10, 11 and 12, saturation indices of ~0.59, 0.62 and 0.66, respectfully, were omitted.

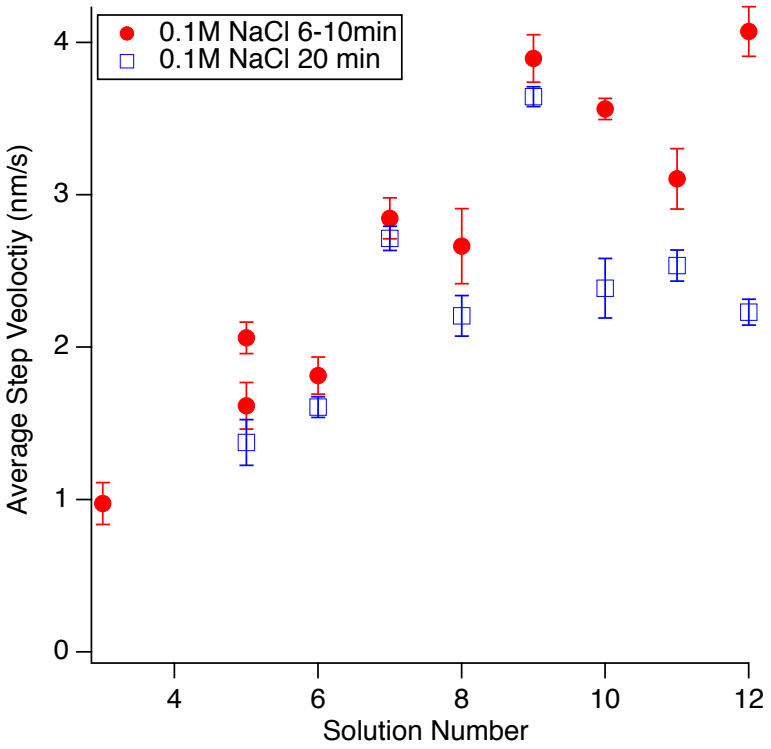

Figure S15: Average Step Velocity (nm/s) versus Solution Number for 0.1 M sodium chloride solutions where data is taken as soon as possible, ~6-10 minutes after solution is switched in and data collected around 20 to 30 minutes after the switch. Solution numbers 10, 11 and 12 should be considered to be omitted due to possible solution stability over time.

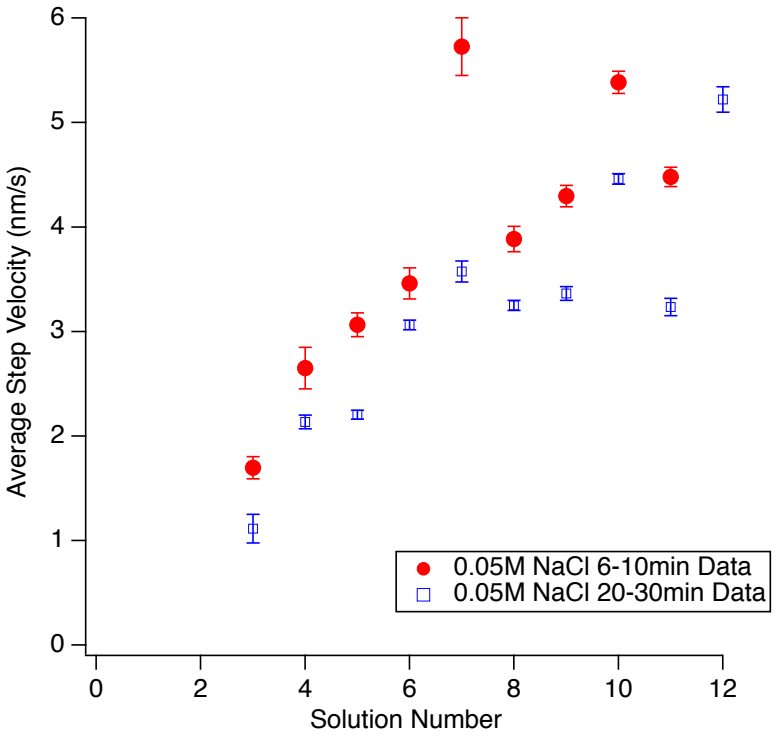

Figure S16: Average Step Velocity (nm/s) versus Barium Activity for 0.05 M sodium chloride solutions where data is taken as soon as possible, ~6-10 minutes after solution is switched in and data collected around 20 to 30 minutes after the switch. 0.05 M sodium chloride solutions show instability, especially solutions 10, 11 and 12. Solutions 10, 11, and 12 should be omitted and solutions 8 and 9 may need to be considered too.

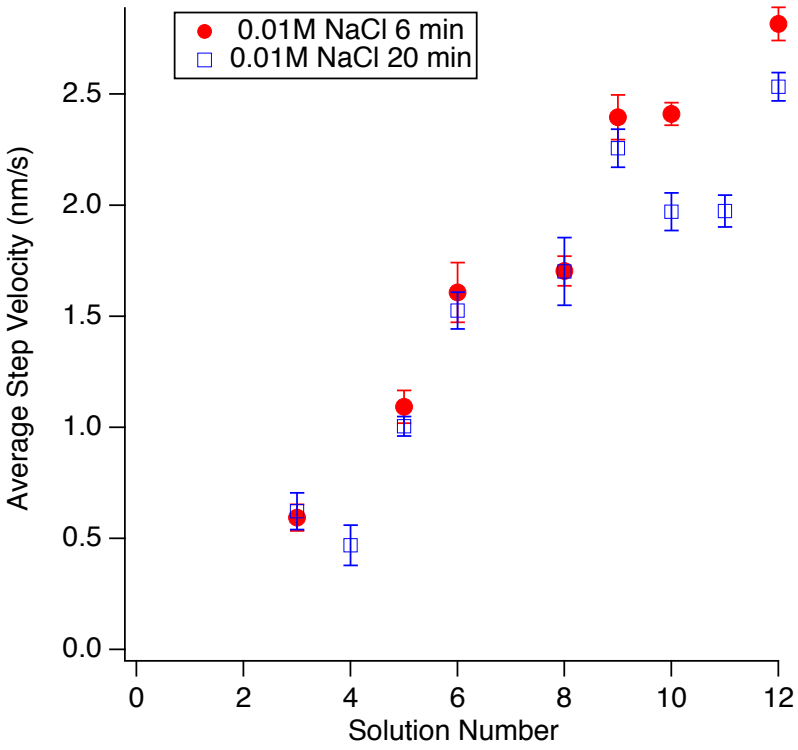

Figure S17: Average Step Velocity (nm/s) versus Barium Activity for 0.01 M sodium chloride solutions where data is taken as soon as possible, ~6-10 minutes after solution is switched in and data collected around 20 to 30 minutes after the switch. Solution numbers 10, 11, and 12 should be considered to be omitted due to possible solution stability over time.

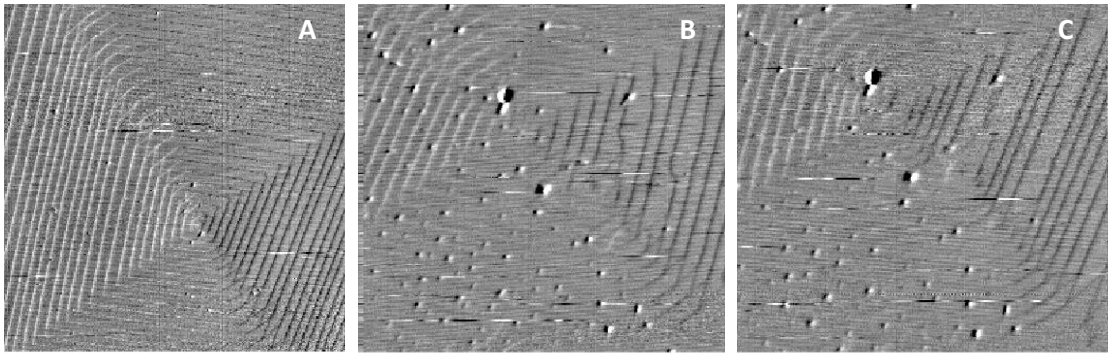

Figure S18: A solution chemistry of 12-ClA A) 11 minutes B) 1.25 hours of growth and C) fresh solution coming in. In C) the step density has increased from image B to image C.

Another indication of issues with solution stability can be shown in the appearance of the top of the hillock. As the solution ages over time, the spacing between steps appear to increase and the step density decreases but when a fresh solution of the same chemistry comes through the fluid cell, there is an apparent increase in step density at the top of the hillock (Figure S18).

Using Figure 2 found in He et al.,[1] solution compositions of 10, 11 and 12-ClA have estimated induction periods of 2, 2.4 and 3.5 hours. This is well within the timing of our experiments. For 10, 11, and 12-ClC the induction time were 4.7, 7.2 and 11.4 hours. He et al. 1995 used a turbidity meter so the induction period could start much earlier but cannot be monitored due to the lack of sensitivity of the meter. These induction times are within the times of the experiments and Figure S15, Figure S16, and Figure S17 show that step velocities decreased over time of solutions 10, 11 and 12 for the three ionic strengths of sodium chloride, showing solution instability. Figure S14 (flow rate test) not only shows that the step velocities are independent of flow rate (mL/hr) but that over the span of the first 15 minutes of data collection, the step velocity decreased by 1.28 nm/s. Additional solution stability testing using more diluted stock solutions of barium chloride and sodium sulfate resulted in the same evidence of solution stability.

Solution Stability of Sodium Nitrate Solutions

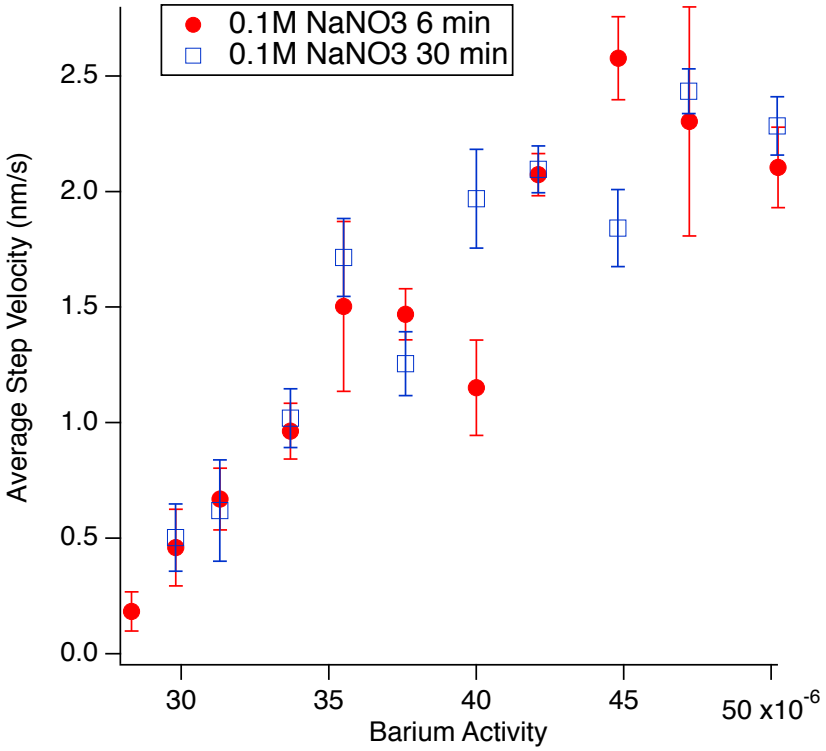

Figure S19: Average Step Velocity (nm/s) versus Barium Activity for 0.1 M sodium nitrate solutions where data is taken as soon as possible, ~6-10 minutes from switch, and when data is collected around 20-30 minutes after the switch. From the data, the 0.1 M sodium nitrate solutions are stable over time and therefore there is no reason to omit any higher supersaturated solutions.

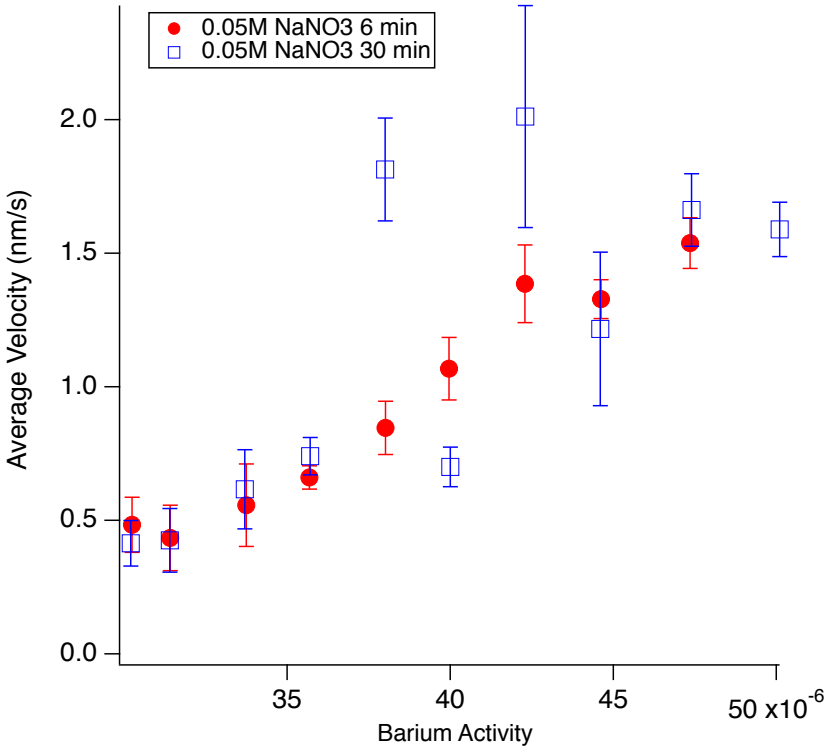

Figure S20: Average Step Velocity (nm/s) versus Barium Activity for 0.05 M sodium nitrate solutions where data is taken as soon as possible, ~6-10 minutes from switch, and when data is taken around 20-30 minutes after the switch. From the data, the 0.05 M sodium nitrate solutions are stable over time and therefore there is no reason to omit any higher supersaturated solutions.

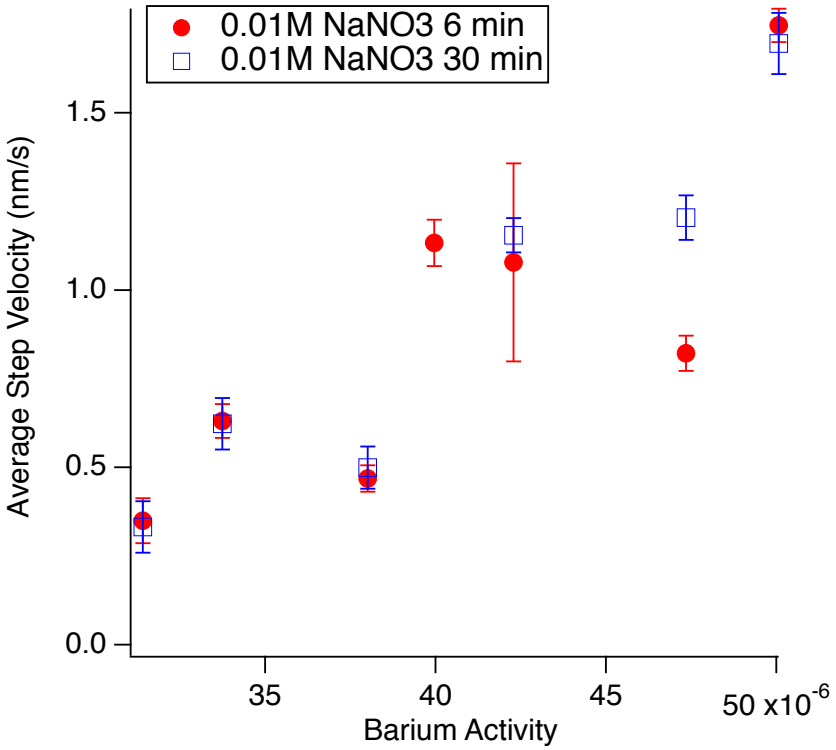

Figure S21: Average Step Velocity (nm/s) versus Barium Activity for 0.01 M sodium nitrate solutions where data is taken as soon as possible, ~6-10 minutes from switch, and when data is taken around 20-30 minutes after the switch. From the data, the 0.01 M sodium nitrate solutions are stable over time and therefore there is no reason to omit any higher supersaturated solutions.

Figure S19, Figure S20, and Figure S21 show that there is no clear evidence of solution instability for sodium nitrate solutions. This could be due to the lower barium activities of the solutions and the ratio at unity compared to higher barium activities and higher ratio of the sodium chloride solutions.

APPENDIX B: References

1. He, S.; Oddo, J.; Tomson, M. The Nucleation Kinetics of Barium-Sulfate in NaCl Solutions Up to 6 M and 90-Degrees-C. *J. Colloid Interface Sci.* **1995**, *174*, 319-326.